Macrophage Innate Training Induced by IL-4 Activation Enhances OXPHOS Driven Anti-Mycobacterial Responses

Mimmi L. E. Lundahl[1,2]*, Morgane Mitermite[3a], Dylan G. Ryan[4,5a], Niamh C. Williams[4], Ming Yang[5], Filipa Lebre[1], Aoife L. Gorman[1], Bojan Stojkovic[3], Christian Frezza[5], Eoin M. Scanlan[2], Luke A. J. O'Neill[4], Stephen V. Gordon[3], Ed C. Lavelle[1,6]*.

[1]School of Biochemistry and Immunology, Adjuvant Research Group, Trinity Biomedical Sciences Institute, Trinity College Dublin, Dublin, D02 R590 Ireland.

[2]School of Chemistry, Scanlan Research Group, Trinity Biomedical Sciences Institute, Trinity College Dublin, Dublin, D02 R590 Ireland.

[3]School of Veterinary Medicine, UCD Veterinary Sciences Centre, University College Dublin, Dublin, Ireland.

[4]School of Biochemistry and Immunology, Inflammation Research Group, Trinity Biomedical Sciences Institute, Trinity College Dublin, D02 R590 Ireland.

[5]Hutchison/MRC Research centre, MRC Cancer Unit, University of Cambridge, Cambridge, CB2 0XZ UK.

[6]Lead contact

[a]Share joint second authorship

*Correspondence: lavellee@tcd.ie and lundahlm@tcd.ie

Abstract

Macrophages are key innate immune cells for determining the outcome of *Mycobacterium tuberculosis* infection. Polarization with IFNγ and LPS into the "classically activated" M1 macrophage enhances pro-inflammatory and microbicidal responses, important for eradicating the bacterium. By contrast, "alternatively activated" M2 macrophages, polarized with IL-4, oppose bactericidal mechanisms and allow mycobacterial growth. These activation states are accompanied by distinct metabolic profiles, where M1 macrophages favor near exclusive use of glycolysis, whereas M2 macrophages up-regulate oxidative phosphorylation (OXPHOS). Here we demonstrate that activation with IL-4 counterintuitively induces protective innate memory against mycobacterial challenge. This was associated with enhanced pro-inflammatory cytokine responses and killing capacity. Moreover, despite this switch towards a phenotype that is more akin to classical activation, IL-4 trained macrophages do not demonstrate M1-typical metabolism, instead retaining heightened use of OXPHOS. Moreover, inhibition of OXPHOS with oligomycin, 2-deoxy glucose or BPTES all impeded heightened pro-inflammatory cytokine responses from IL-4 trained macrophages. Lastly, this work identifies that IL-10 negatively regulates protective IL-4 training, impeding pro-inflammatory and bactericidal mechanisms. In summary, this work provides new and unexpected insight into alternative macrophage activation states in the context of mycobacterial infection.

Introduction

Mycobacterium tuberculosis, the causative agent of tuberculosis (TB), has arguably caused the most deaths of any pathogen in human history. *M. tuberculosis* continues to be the cause of more than a million deaths annually: in 2018, 10 million people were newly diagnosed with active TB and 1.4 million died from the disease (WHO, 2019). The only currently licensed TB vaccine, Bacille Calmette-Guérin (BCG), was developed a century ago and although it protects children against disseminated disease, it fails to protect adults from pulmonary infection (Ryndak & Laal, 2019). The lack of an efficient vaccine, and growing antibiotic resistance, means that new ways of combatting TB are urgently needed (Choreño-Parra, Weinstein, Yunis, Zúñiga, & Hernández-Pando, 2020).

Macrophages are key host innate immune cells for controlling *M. tuberculosis* infection (Cohen et al., 2018). A significant feature of macrophages is dynamic plasticity, expressed by their ability to polarize towards distinct activation states (M. L. E. Lundahl, Scanlan, & Lavelle, 2017; Sica, Erreni, Allavena, & Porta, 2015). Activation with interferon gamma (IFNγ) together with lipopolysaccharides (LPS) yields the bactericidal and pro-inflammatory "classically activated" or M1 macrophages (Ferrante & Leibovich, 2012; Sica et al., 2015), whereas activation with the type 2 and regulatory cytokines, interleukin (IL)-4, IL-13, IL-10 and transforming growth factor (TGF)β, results in "alternatively activated" M2 macrophages, which enhance allergic responses, resolve inflammation and induce tissue remodeling (Bystrom et al., 2008; Mantovani et al., 2004). Another key difference between these activation states are their metabolic profiles: whereas classically activated macrophages switch to near exclusive use of glycolysis to drive their ATP production, alternatively activated macrophages instead upregulate their oxidative phosphorylation (OXPHOS) machinery (Van den Bossche et al., 2016; Van den Bossche, O'Neill, & Menon, 2017).

Whilst classifying macrophages in this manner is a simplification – the reality is a broad spectrum of various differentiation states that is continuously regulated by a myriad of signals (Sica et al., 2015) – it is nevertheless considered that for a host to control TB infection, classical macrophage activation is vital (Jouanguy et al., 1999; Philips & Ernst, 2012). Furthermore, a macrophage metabolic shift to glycolysis is crucial for effective killing and thus overall control of TB infection (Gleeson et al., 2016; Huang, Nazarova, Tan, Liu, & Russell, 2018). By contrast, alternatively activated macrophages directly oppose bactericidal responses, which has been demonstrated to lead to enhanced bacterial burden and TB pathology (Moreira-Teixeira et al., 2016; Orecchioni, Ghosheh, Pramod, & Ley, 2019; Shi, Jiang, Bushkin, Subbian, & Tyagi, 2019). Due in large part to the established ability of classically activated macrophages to kill *M. tuberculosis*, inducing Th1 immunity is a key aim for TB vaccine development (Abebe, 2012; Andersen & Kaufmann, 2014; Ottenhoff et al., 2010). Apart from targeting adaptive immune memory, another promising approach has emerged in recent years: bolstering

innate immune killing capacity by the induction of innate training (Khader et al., 2019; Moorlag et al., 2020).

Innate training is regarded as a form of immunological memory. It is a phenomenon where a primary challenge, such as a vaccination or an infection, induces epigenetic changes in innate immune cells, which alters their responses following a secondary challenge (Arts et al., 2018; Saeed et al., 2014; van der Meer, Joosten, Riksen, & Netea, 2015). Unlike adaptive immune memory, innate training is non-specific, i.e. the secondary challenge does not need to be related to the primary challenge. For instance, BCG vaccination has been demonstrated to protect severe combined immunodeficiency (SCID) mice from lethal *Candida albicans* infection; reducing fungal burden and significantly improving survival (Kleinnijenhuis et al., 2012). This ability of the BCG vaccine to train innate immunity is now believed to be a core mechanism by which it induces its protection against *M. tuberculosis*. Apart from the BCG vaccine, it has been demonstrated that other organisms and compounds can induce innate training, such as β-glucan (van der Meer et al., 2015) which induced protective innate training against virulent *M. tuberculosis*, as shown by enhanced mouse survival following *in vivo* infection, and enhanced human monocyte pro-inflammatory cytokine secretion following *ex vivo* infection (Moorlag et al., 2020).

Conversely, there is a risk that certain immune challenges could lead to innate immune re-programming that hinders protective immune responses. For instance, recent reports have demonstrated how virulent *M. tuberculosis* (N. Khan et al., 2020) and mycobacterial phenolic glycans (M. Lundahl et al., 2020) can program macrophages to attenuate bactericidal responses to subsequent mycobacterial challenge. In the current study, macrophage activation caused by former or concurrent parasitic infections is considered regarding the possibility of innate immune re-programming that hinders protective immune responses against this disease. Geographically, there is extensive overlap between tuberculosis endemic areas and the presence of helminths (Salgame, Yap, & Gause, 2013). With regard to macrophage activation and combatting tuberculosis, this is an issue as parasites induce type 2 responses, leading to alternative macrophage activation instead of classical activation and associated bactericidal responses (Chatterjee et al., 2017; X. X. Li & Zhou, 2013). Indeed, it was recently demonstrated how products of the helminth *Fasciola hepatica* can train murine macrophages for enhanced secretion of the anti-inflammatory cytokine IL-10 (Quinn et al., 2019).

Unexpectedly, our data indicates that murine macrophage activation with IL-4 and IL-13 induces innate training that enhances pro-inflammatory and bactericidal responses against mycobacteria. Although macrophages trained with IL-4 and IL-13 resemble classically activated macrophages, we identify that they do not adopt their typical metabolic profile, instead retaining heightened OXPHOS activity and notably lacking a dependency on glucose and glycolysis. Lastly, we

identify IL-10 as a negative regulator of this innate training response, which may have obscured previous identification of this macrophage phenotype.

Results

Prior Alternative Activation Enhances Mycobacterial Killing

Macrophages are key immune cells for combatting *M. tuberculosis*. Upon infection, alveolar macrophages serve as the initial hosts of the intracellular bacterium (Cohen et al., 2018) and bactericidal responses of recruited monocyte-derived macrophages (MDM) are crucial for control and killing of *M. tuberculosis* (Huang et al., 2018). Overall, it has been highlighted that an early Th1 driven immune response is key to early eradication of *M. tuberculosis*, where classical activation of macrophages results in effective bactericidal action. However, a complicating factor is the occurrence of concurrent parasitic disease, which instead drives Th2 immunity and alternative macrophage activation, which in turn has been demonstrated to enhance TB pathology (Moreira-Teixeira et al., 2016; Orecchioni et al., 2019). In this context, we sought to investigate how type 2 responses may induce innate memory, and how such memory could affect macrophage bactericidal properties.

To investigate the effect of IL-4 and IL-13 on macrophage acute and innate memory responses, an *in vitro* model of BCG infection was used. Murine bone marrow-derived macrophages (BMDMs) were stimulated with IL-4 and IL-13 (M(4/13)) on Day -1, followed by infection with BCG Denmark on either Day 0 or Day 6 (**Figure 1A**). On either day, the macrophages were exposed to roughly 30 bacteria per cell and after three hours extracellular bacteria were removed by washing and internalized bacteria were measured by colony forming units (CFUs), resulting in a multiplicity of infection (MOI) between one and four, depending on differences in uptake (**Figure 1B**). Internalized bacteria were measured by CFU (**Figure S1A**) at 27- and 51 hours post infection to determine killing capacity (**Figure 1C**).

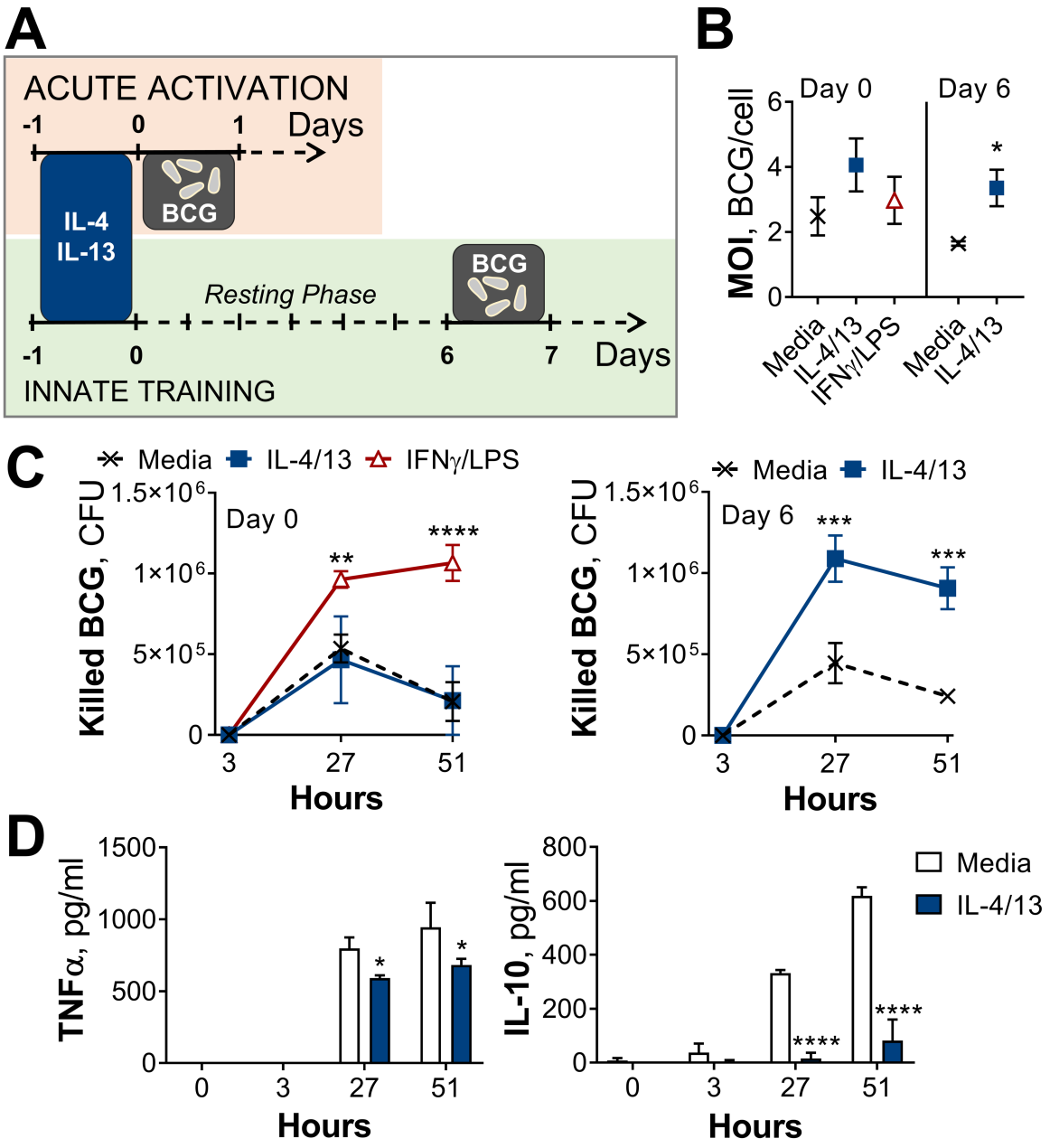

Figure 1. Training with IL-4 and IL-13 enhances BMDM mycobacterial killing capacity.

(**A**) Schematic of protocol for BCG infection following acute activation (Day 0) or training (Day 6) with IL-4 and IL-13. (**B-C**) BCG Denmark MOI (B) and killing after h as indicated (C), measured by CFU per 0.5×10^6 BMDMs on Day 0 or Day 6. BMDMs were incubated with media, IL-4 with IL-13 or IFNγ with LPS for 24 h on Day -1. (**D**) Secretion of indicated cytokines from BMDMs treated as in (C), standardized to 0.5×10^6 BMDMs. (B-D) Representative results (n = 2) showing mean ± SEM (B-C) or ± STD (D) and analyzed by student's t-test (B) or multiple t-tests, with Holm-Sidak correction (C-D), compared with media control. * $p \leq 0.05$, ** $p \leq 0.01$, **** $p \leq 0.0001$.

Mycobacterial killing was compared to naïve BMDMs incubated with media on day -1 (media control, M(-)) on both Days 0 and 6, and BMDMs classically activated with IFNγ and LPS (M(IFNγ/LPS)) on Day 0. M(IFNγ/LPS) could not be investigated on Day 6 due to reduced viability. On Day 0, M(IFNγ/LPS) displayed significantly enhanced mycobacterial killing at 27- and 51-hours post infection, whereas

M(4/13) displayed comparable killing capacity to naïve M(-) (**Figure 1C**). Secretion of TNFα and IL-10 were also measured at 3-, 27- and 51 hours post infection on Day 0 (**Figure S1B**) and Day 6 (**Figure 1D**). These cytokines were chosen as TNFα is critical in the early host response against *M. tuberculosis* (Bourigault et al., 2013; Keane et al., 2001), while IL-10 can prevent phagolysosome maturation in human macrophages (O'Leary, O'Sullivan, & Keane, 2011) and promote disease progression in mice (Beamer et al., 2008). Following BCG infection on Day 0 (**Figure S1B**), IL-10 was not detectable and bactericidal M(IFNγ/LPS) secreted TNFα. Consistent with previous work, activation with IL-4 and IL-13 on the other hand did not enhance BCG killing nor induce inflammatory cytokine secretion.

By contrast, on Day 6 (innate training responses), M(4/13) exhibited both heightened mycobacterial uptake (**Figure 1B**) and significantly greater killing capacity compared with untrained M(-), both at 27- and 51 hours post infection (**Figures 1C** and **S1A**). Furthermore, this was accompanied by a near complete abrogation of IL-10 secretion, along with a minor decrease of TNFα compared with M(-) (**Figure 1D**), displaying an overall shift towards a more pro-inflammatory response profile. To investigate the change in phenotype of M(4/13) between the two days tested, a more detailed characterization was carried out.

Innate Training with IL-4 and IL-13 Promotes Pro-Inflammatory Responses

The current dogma suggests that classical (M1) macrophage activation induces upregulation of antigen presentation, enhanced secretion of pro-inflammatory cytokines including interleukin (IL)-1β, IL-6 and TNFα, as well as the production of reactive oxygen and nitrogen species (ROS and RNS respectively) (Bystrom et al., 2008; Sica et al., 2015). By contrast, alternatively activated macrophages (M2) dampen inflammation, promote angiogenesis and scavenge debris (Gordon & Martinez, 2010; Sica et al., 2015). These macrophages are identified by their upregulation of chitinase-like 3-1 (Chil3), found in inflammatory zone-1 (Fizz1, Retnla) and arginase (Arg1) (Gabrilovich, Ostrand-Rosenberg, & Bronte, 2012; Murray & Wynn, 2011), as well as surface expression of lectins, such as the macrophage mannose receptor (MR, CD206) (Brown & Crocker, 2016). Flow cytometry and qPCR analysis of M(IFNγ/LPS) and M(4/13), compared with inactivated M(-), showed that these activation phenotypes tallied with the literature: M(IFNγ/LPS) had elevated expression of CD80, major histocompatibility complex class II (MHC II) and inducible nitric oxide synthase (iNOS, *Nos2*) – responsible for production of the reactive nitrogen species, nitric oxide (NO) – whereas M(4/13) exhibited heightened expression of CD206, MHC II, *Arg1*, *Chil3* and *Retnla* (**Figures S2A-C**).

To examine their respective cytokine response profiles, M(IFNγ/LPS) and M(4/13) were stimulated with killed *M. tuberculosis* strain H37Rv (hereafter referred to as Mtb) or the TLR1/2 ligand tripalmitoyl-*S*-glyceryl-cysteine (PAM3CSK4) on either Day 0 or Day 6. Acutely activated M(IFNγ/LPS) demonstrated elevated secretion of TNFα, IL-6 and IL-10 in response to Mtb (**Figure S2D**) and elevated

TNFα and IL-6 in response to PAM3CSK4 (**Figure S3A**), compared with M(-). By contrast, M(4/13) had attenuated secretion of each cytokine compared with M(-), following either Mtb or PAM3CSK4 stimulation. However, on Day 6 (innate memory responses), both M(IFNγ/LPS) and M(4/13) secreted greater pro-inflammatory TNFα and reduced anti-inflammatory IL-10 in response to Mtb (**Figure 2A**), and secreted elevated TNFα following PAM3CSK4 stimulation (**Figure S3B**). M(4/13) additionally exhibited increased IL-6 secretion in response to both stimuli. As with the BCG infection, M(IL-4/13) responses changed markedly between Day 0 and Day 6, shifting towards a pro-inflammatory response profile which was similar to classically activated macrophages.

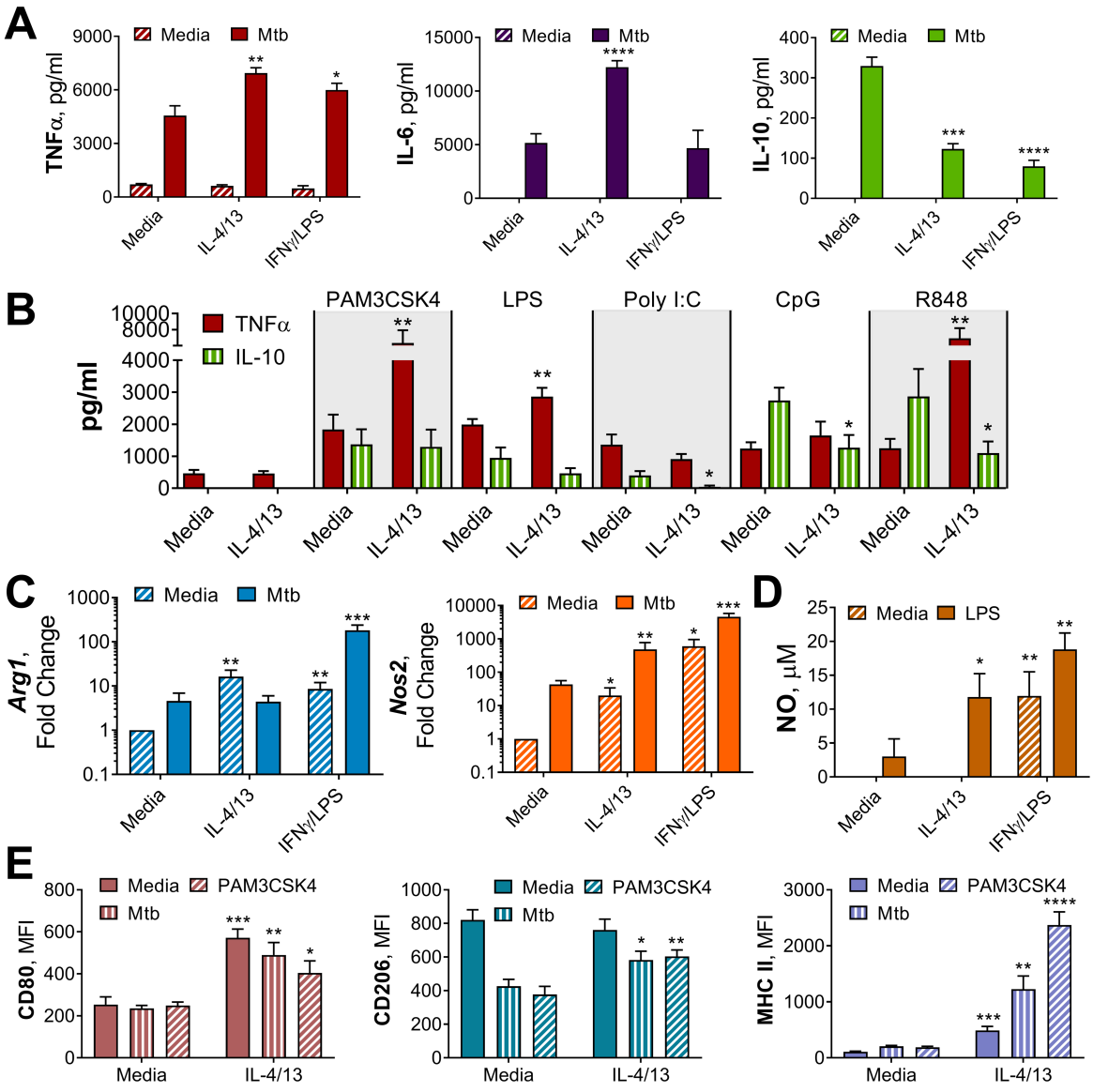

Figure 2. Innate training of BMDMs with IL-4 and IL-13 enhances pro-inflammatory responses.

(**A-B**) Cytokine secretion following BMDM 24 h incubation with irradiated *M. tuberculosis* (Mtb) (A), TLR agonists (B) or media on Day 6 as indicated. BMDMs were previously incubated with media, IL-4 with IL-13 or IFNγ with LPS on Day -1 for 24 h (n = 3). (**C**) qPCR of indicated mRNA in BMDMs treated as in (A), standardized to BMDMs incubated with media Day -1 and Day 6 (n = 4). (**D**) Nitric oxide (NO) secretion from BMDMs treated as in (B) (n = 3). (**E**) Expression of CD80, CD206 and MHC II (gating strategy Figure S2A) on BMDMs treated as in (A-B) (n = 3). Mean ± SD are shown and analyzed by student's t-test, compared with media control. * $p \leq 0.05$, ** $p \leq 0.01$, *** $p \leq 0.001$, **** $p \leq 0.0001$.

To consider whether the shift in M(4/13) to a pro-inflammatory cytokine profile was dependent on epigenetic changes, the DNA methylation inhibitor 5'-deoxy-5'-(methylthio)adenosine (MTA), was employed. This inhibitor has been demonstrated to impede training by BCG (Kleinnijenhuis et al., 2012) and β-glucan (Quintin et al., 2012) – which promote pro-inflammatory responses – as well as training induced by helminth *Fasciola hepatica* total extract (Quinn et al., 2019), which enhances anti-inflammatory responses such as IL-10 and IL-1Ra secretion. The addition of MTA prior to activation

with IL-4 and IL-13 on day -1 reduced TNFα, IL-6 and IL-10 secretion induced by either Mtb or PAM3CSK4 on Day 6 (**Figure S3C**), resulting in a profile reminiscent of acutely activated M(4/13) (**Figure S2D**). By contrast, inhibition of DNA methylation in M(-) resulted in comparable or even increased cytokine secretion. This suggested that DNA methylation following IL-4 and IL-13 activation contributed to the innate training and subsequent enhancement of pro-inflammatory responses.

Next, we addressed whether the shift towards pro-inflammatory responses was applicable to other stimuli, trained M(4/13) were incubated with various Toll-like receptor (TLR) agonists on Day 6 (**Figure 2B**). Incubation of cells with ligands for TLR1/2, TLR4, TLR7/8 or TLR 9 resulted in an increase of TNFα production, reduced IL-10 secretion or both. This demonstrated that prior activation with IL-4 and IL-13 caused a subsequent shift towards a pro-inflammatory response profile in response to a range of pathogen-related agonists.

Having considered cytokine responses, the expression of *Arg1* and *Nos2* and the secretion of NO were next addressed. In mice, the induction of iNOS is important for bactericidal NO production and subsequent killing of *M. tuberculosis* (Flynn et al., 1993; Pasula, Martin, Kesavalu, Abdalla, & Britigan, 2017). In turn, Arg1 directly impedes the bactericidal function of iNOS by sequestering the amino acid, arginine, which each enzyme uses to make their respective products: ornithine and NO. Subsequently, in the murine model of TB infection, Arg1 has been linked with increased bacterial burden and pathology (Moreira-Teixeira et al., 2016).

Without a secondary stimulation on Day 6, M(4/13) and M(IFNγ/LPS) displayed higher levels of *Arg1* and *Nos2* expression, compared with BMDMs incubated in media alone (**Figure 2C**), and M(IFNγ/LPS) exhibited markedly higher expression of *Nos2* compared with M(4/13). Following stimulation with Mtb (**Figure 3C**) or PAM3CSK4 (**Figure S3D**) M(IFNγ/LPS) exhibited elevated expression of both *Arg1* and *Nos2* compared with untrained M(-), however the trained M(4/13) exhibited equivalent expression of *Arg1*, but with enhanced *Nos2*, demonstrating a further shift towards an M1 profile. An increase in NO production could not be detected following Mtb stimulation; however, following LPS stimulation, both M(4/13) and M(IFNγ/LPS) secreted greater levels of NO compared to M(-) (**Figure 2D**).

Other M1 and M2 markers were analyzed by flow cytometry, following incubation with media, Mtb or PAM3CSK4 on Day 6 (**Figure 2E**). Without secondary stimulation, M(4/13) exhibited an M1-typical profile: heightened expression of CD80 and MHC II, whilst CD206 expression was comparable to M(-). Following secondary stimulation with either Mtb or PAM3CSK4, M(4/13) CD80, CD206 and MHC II expression was significantly greater compared with M(-). Having observed a change in activation markers, cytokine induction and bactericidal capacity in M(4/13) between Days 0 and 6, the next question was whether there was a corresponding shift in glycolytic metabolism.

240

241 **BMDMs Trained with IL-4 and IL-13 Retain OXPHOS Metabolism**

242 The increased energy and biosynthetic precursor demand induced by various macrophage activation
243 states are met in distinct ways. Consistent with previous studies, M(4/13) on Day 1 displayed both an
244 increase of oxygen consumption rate (OCR) – indicative of mitochondrial OXPHOS activity – and
245 extracellular acidification rate (ECAR) – an indirect measurement of lactic acid secretion and thus
246 indicative of glycolysis (**Figure 3A**). This demonstrated how alternative activation is intrinsically linked
247 with enhanced mitochondrial OXPHOS activity, via the tricarboxylic acid (TCA) cycle (Van den Bossche
248 et al., 2016; Wang et al., 2018). The TCA cycle is in turn driven by glycolysis, glutaminolysis and fatty
249 acid oxidation (Viola, Munari, Sánchez-Rodríguez, Scolaro, & Castegna, 2019). By contrast, acutely
250 activated M(IFNγ/LPS) displayed an increase in ECAR and reduced OCR (**Figure 3A**), which was
251 indicative of augmented glycolysis to meet the increased need for ATP, whilst ATP synthesis via
252 OXPHOS is hindered (Liu et al., 2016). This glycolytic shift is critical for pro-inflammatory responses
253 induced by classically activated macrophages and moreover results in mitochondrial dysfunction (Van
254 den Bossche et al., 2016).

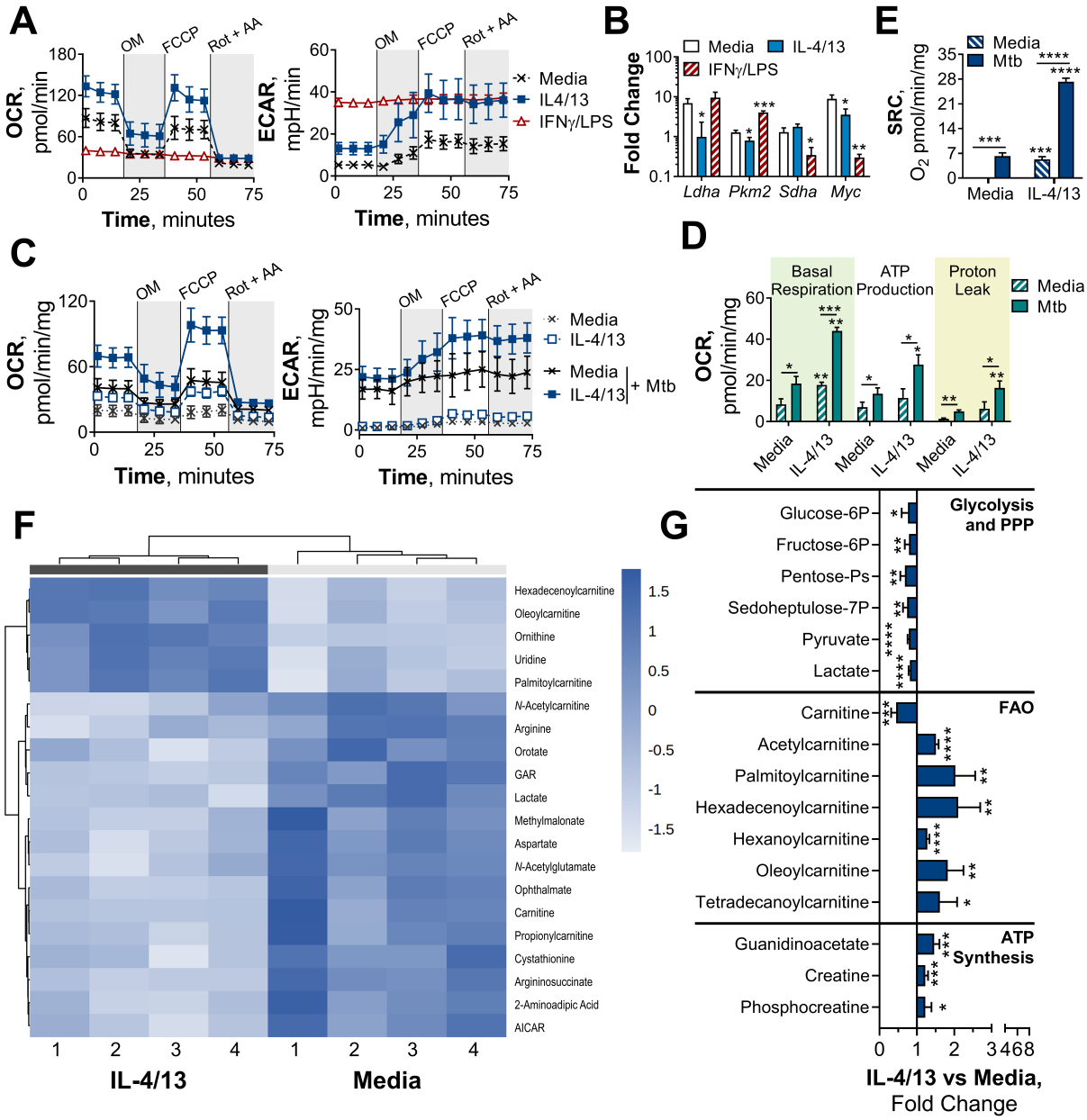

Figure 3. BMDMs trained with IL-4 and IL-13 retain M2-typical metabolism upon mycobacterial challenge.

(**A**) Extracellular flux analysis of BMDMs, following 24 h incubation with IL-4 and IL-13, IFNγ and LPS or media (n = 2). (**B**) qPCR of indicated mRNA in BMDMs following incubation with media, IL-4 with IL-13 or IFNγ with LPS for 24 h on Day -1 and stimulated with irradiated *M. tuberculosis* (Mtb) for 6 h (*Pkm2*) or 24 h (*Ldha*, *Sdha* and *Myc*), standardized to BMDMs given media on Day -1 and Day 6 (n = 3). (**C-E**) Extracellular flux analysis (C), basal respiration, ATP production, proton leak (D) and spare respiratory capacity (SRC) (E) of BMDMs treated as in (B), with incubation with media or IL-4 with IL-13 on Day -1 and stimulation with media or Mtb for 24 h on Day 6 (n = 3). (**F-G**) Metabolites from BMDMs treated as in (B), incubated with media or IL-4 with IL-13 on Day -1 and stimulation with Mtb for 24 h on Day 6 (n = 4). MetaboAnalyst generated heatmap representing hierarchical clustering of the top 20 most up/down regulated metabolites (F). Fold change compared with media control (=1) (G). Mean ± SD are shown and analyzed by student's t-test. * $p \leq 0.05$, ** $p \leq 0.01$, *** $p \leq 0.001$, **** $p \leq 0.0001$. Abbreviations: AA, antimycin-A; AICAR, aminoimidazole carboxamide ribonucleotide; ECAR, extracellular acidification rate; FAO, fatty acid oxidation; GAR, glycinamide ribonucleotide; OCR, oxygen consumption rate; P, phosphate; PPP, pentose phosphate pathway; Rot, rotenone.

Due to the link between glycolysis and classical activation, it is not surprising that prior work has proposed that a macrophage glycolytic shift is crucial for effective killing and thus overall control of TB infection (Gleeson et al., 2016; Huang et al., 2018). Furthermore, it has recently been proposed that *M. tuberculosis* impedes this glycolytic shift as an immune evasion strategy (Hackett et al., 2020). As we had observed that innate memory responses induced by IL-4 and IL-13 caused a switch towards a pro-inflammatory and bactericidal response profile, akin to a classically activated macrophage, it was pertinent to address whether there was an accompanying glycolytic shift. Previous work by Van den Bossche et al. has highlighted that because IL-4 activated human MDMs retain their metabolic versatility, they are able to be "re-polarized" to a classical phenotype (Van den Bossche et al., 2016). This was demonstrated by activating MDMs for 24 hours with IL-4, before the cells were washed and re-stimulated with IFNγ and LPS for another 24 hours. MDMs previously activated with IL-4 secreted higher concentrations of TNFα, IL-6 and IL-12 compared with MDMs that were naïve prior to IFNγ and LPS stimulation. This adaptive quality to re-polarize is restricted to alternatively activated macrophages, as mitochondrial dysfunction in classically activated macrophages prevents them from re-polarizing to an alternative phenotype (Van den Bossche et al., 2016). Subsequently, we next addressed whether the IL-4 trained macrophages were adopting a metabolic profile similar to a classical macrophage, or retaining their more versatile metabolic profile.

As with the BCG infection studies, due to the reduced viability of the M(IFNγ/LPS) by Day 6 and 7, OCR and ECAR measurements did not reach the detection limit. To compare metabolic phenotypes of the trained macrophages at these later time points, transcription profiles were therefore analyzed. Prior work has established that the transcription factor hypoxia-inducible factor-1 alpha (HIF-1α) aids the glycolytic metabolic shift following classical activation, such as upregulating the enzyme lactate dehydrogenase (LDH) (Seth et al., 2017) to increase lactic acid fermentation. Tallying with these studies, trained M(IFNγ/LPS) on Day 7 exhibited elevated expression of LDH (*Ldha*) and pyruvate kinase isozyme M2 (PKM2, *Pkm2*) (**Figure S4A**). PKM2 has been shown to play a key role in stabilizing HIF-1α and is thus a crucial determinant for glycolytic metabolism re-wiring (Palsson-McDermott et al., 2015). By contrast, on Day 7, M(4/13) displayed a similar level of LDH expression and reduced transcription of PKM2 compared with M(-).

On the other hand, considering OXPHOS machinery at this time point, trained M(IFNγ/LPS) showed reduced expression of the TCA cycle enzyme succinate dehydrogenase (SDH, *Sdha*), whereas this downregulation was not present in M(4/13) (**Figure S4A**). Moreover, M(4/13) and M(IFNγ/LPS) respectively displayed increased and decreased expression of the transcription factor myelocytomatosis viral oncogene (c-Myc, *Myc*). IL-4 and IL-13 induce c-Myc expression in alternatively

activated macrophages (L. Li et al., 2015; Luiz et al., 2020) and contrastingly LPS induced upregulation of HIF-1α occurs in tandem with downregulation of c-Myc (Liu et al., 2016). Overall, without secondary stimulation, both trained M(IFNγ/LPS) and M(4/13) retained transcriptional and metabolic profiles consistent with previous reports.

Upon secondary stimulation on Day 6 with either Mtb (**Figure 3B**) or PAM3CSK4 (**Figure S4B**), M(IFNγ/LPS) maintained the elevated expression of *Pkm2*, accompanied by reduced transcription of *Sdha* and *Myc*. *Myc* expression was induced in untrained M(-) and M(4/13) by both secondary stimuli, although Mtb did not enhance *Myc* in M(4/13) to the same extent as M(-). Regarding glycolytic metabolism, M(4/13) displayed relatively reduced *Ldha* upon Mtb incubation (**Figure 3B**) and further maintained a similar level of *Sdha* compared with M(-). These results indicated that trained M(IFNγ/LPS) and M(4/13) maintained their respective metabolic profiles following secondary stimulation with Mtb or PAM3CSK4. As such, these results indicated again that trained M(IFNγ/LPS) and M(IL-4/13) maintained their respective metabolic profiles following secondary stimulation with Mtb or PAM3CSK4.

That trained M(4/13) retain OXPHOS metabolism was furthermore supported by Mtb stimulation increasing both OCR and ECAR in M(-) and M(4/13) (**Figure 3C**), where M(4/13) displayed significantly greater OXPHOS driven basal respiration, ATP production and concomitant proton leakage compared with M(-) (**Figure 3D**). In addition, in response to either Mtb (**Figure 3E**) or PAM3CSK4 (**Figure S4C**) there was an increase in spare respiratory capacity (SRC), further signifying that trained M(4/13) retain and even elevate OXPHOS metabolism following secondary stimulation with Mtb.

To further investigate the metabolic profile of trained M(IL-4/13) vs untrained (media control) stimulated with Mtb, the relative change of intracellular metabolite abundance was furthermore assessed by liquid chromatography-mass spectrometry (LC-MS, **Figures 3F-G** and **S4D-E**). This semi-targeted analysis revealed that the trained M(4/13) appeared to have increased use of the urea cycle, as shown by reduced aspartate, arginine and argininosuccinate levels along with enhanced ornithine (**Figure S4E**). Furthermore, there were reduced levels of metabolites associated with glycolysis and the pentose phosphate pathway (PPP) – such as lactate and sedoheptulose-7-phosphate – whilst metabolites involved in fatty acid oxidation (FAO) and ATP synthesis regulation were enhanced (**Figure 3G**). In the case of FAO, reduced carnitine with enhanced carnitine-bound fatty acids (acyl carnitines) signified that fatty acids were being ferried by carnitine into the mitochondrion for FAO. FAO is upregulated during murine M2 macrophage activation and results in the production of acetyl-CoA, NADH and $FADH_2$, which are further used to fuel the TCA cycle and downstream OXPHOS (O'Neill, Kishton, & Rathmell, 2016). Furthermore, the upregulation of creatine and phosphocreatine – as well

as creatine biosynthesis precursor guanidinoacetate – intimated enhanced ATP synthesis. Creatine reacts with ATP to form ADP and phosphocreatine, transporting ATP out of the mitochondrion and preventing allosteric inhibition of ATP synthesis. In the trained M(4/13) the amount of phosphocreatine per ATP was enhanced (**Figure S4F**), which indicated enhanced mitochondrial ATP synthesis and supported the hypothesis that OXPHOS was enhanced. Overall, these results suggested the trained M(4/13) were upregulating their OXPHOS activity in response to mycobacterial challenge.

Having observed that trained M(IL-4/IL-13) showed a distinct metabolic profile from classically activated macrophages, the roles of glycolysis and OXPHOS in driving cytokine production were next investigated with the use of inhibitors. Incubation with the glycolysis and OXPHOS inhibitor 2-deoxy glucose (2-DG) (Wang et al., 2018) prior to stimulation with Mtb (**Figure S5A**) significantly reduced TNFα secretion in M(IFNγ/LPS) and M(-). 2-DG also reduced PAM3CSK4 induced TNFα in M(4/13) and M(IFNγ/LPS) (**Figure S5B**) and reduced IL-6 secretion in M(4/13) following either Mtb or PAM3CSK4 stimulation. Secretion of anti-inflammatory IL-10 following Mtb stimulation was also reduced by 2-DG in M(IFNγ/LPS) and M(4/13). This demonstrated that glycolysis, OXPHOS or both were involved in driving cytokine responses to Mtb and PAM3CSK4 in all tested macrophages.

To further examine the role of OXPHOS, the ATP-synthase inhibitor oligomycin (OM) and the glutaminase inhibitor bis-2-(5-phenylacetamido-1,3,4-thiadiazol-2-yl)ethyl sulfide (BPTES) were used prior to secondary stimulation. The role of glutaminolysis in the trained M(IL-4/13) was of interest, as it has previously been highlighted to compensate for inhibition of glycolysis and fuel the TCA cycle during IL-4 induced macrophage activation (Wang et al., 2018). In the trained M(4/13), inhibition of either OXPHOS or glutaminolysis significantly reduced TNFα and IL-6 secretion following stimulation with either Mtb (**Figure 4A**) or PAM3CSK4 (**Figure S5B**), suggesting that both processes helped drive pro-inflammatory responses. By contrast, in trained M(IFNγ/LPS), although the markedly lower level of IL-6 was further impeded by either inhibitor, the secretion of TNFα was unaffected, supporting M(IFNγ/LPS) use of glycolysis to drive pro-inflammatory responses. OM and BPTES furthermore impeded IL-10 secretion from M(IFNγ/LPS), whereas OM reduced IL-10 secretion in M(4/13) and BPTES did not (**Figure 4A**). In the case of trained M(4/13) this implicated that glutamine metabolism was selectively a driver of pro-inflammatory cytokine responses.

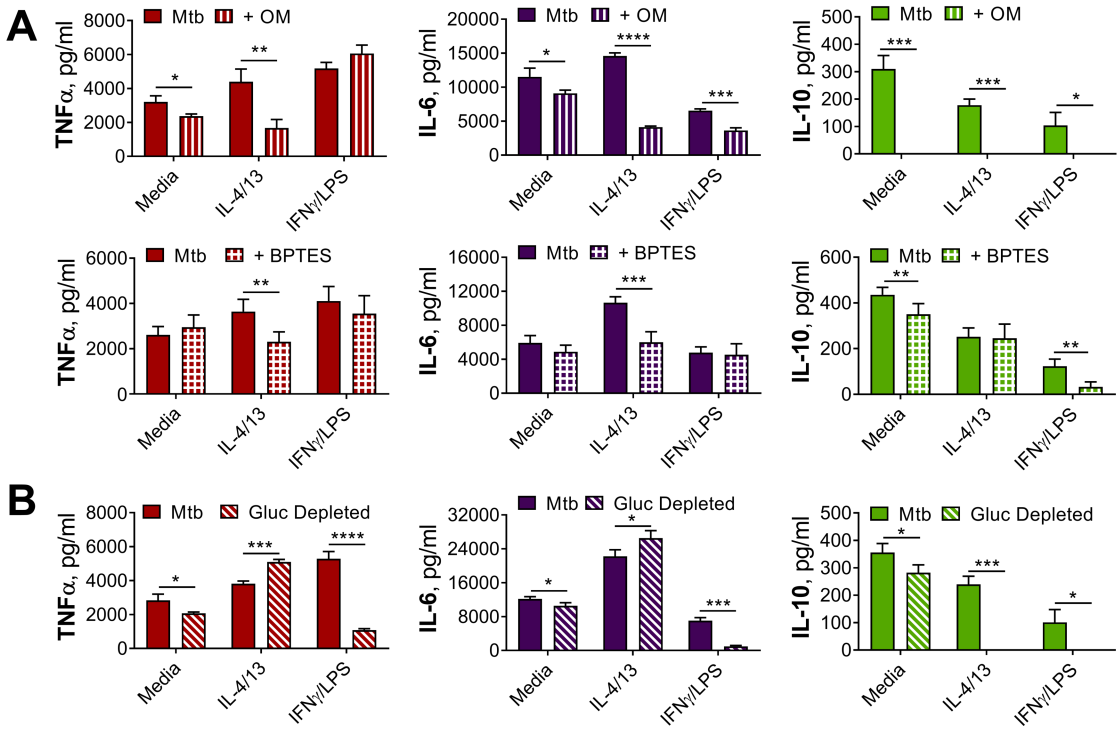

Figure 4. OXPHOS drives inflammatory cytokine responses in IL-4/13 trained BMDMs.

(**A**) Cytokine secretion from BMDMs following incubation with media, IL-4 with IL-13 or IFNγ with LPS for 24 h on Day -1 and incubation with irradiated *M. tuberculosis* (Mtb) on Day 6 for 24 h, with or without pre-incubation (Day 6) of oligomycin (OM) or BPTES (n = 4). (**B**) Cytokine secretion from BMDMs treated as in (A), with or without glucose depleted conditions between Day -1 to 7 (n = 3). Mean ± SD are shown and analyzed by student's t-test as indicated. * $p \leq 0.05$, ** $p \leq 0.01$, *** $p \leq 0.001$, **** $p \leq 0.0001$.

To further cement the differences in glycolytic metabolism between trained M(IFNγ/LPS) and M(4/13), an experiment was carried out where BMDMs were incubated in either glucose depleted media or regular glucose-rich media from Day-1 (**Figure 4B**). Whereas glucose depletion significantly reduced the secretion of TNFα, IL-6 and IL-10 from M(IFNγ/LPS) and M(-), following Mtb stimulation on Day 6, glucose depletion did not impair pro-inflammatory cytokine secretion of M(4/13); instead the secretion of both TNFα and IL-6 was elevated under these conditions, whilst levels of regulatory IL-10 were further reduced, displaying an even greater shift towards pro-inflammatory responses. Furthermore, stimulation with PAM3CSK4 yielded similar results (**Figure S5C**), although IL-6 secretion remained unaltered. This highlighted that although trained M(IFNγ/LPS) and M(4/13) had similar response profiles, M(4/13) appeared to retain M2-typical metabolism (**Figure 5**).

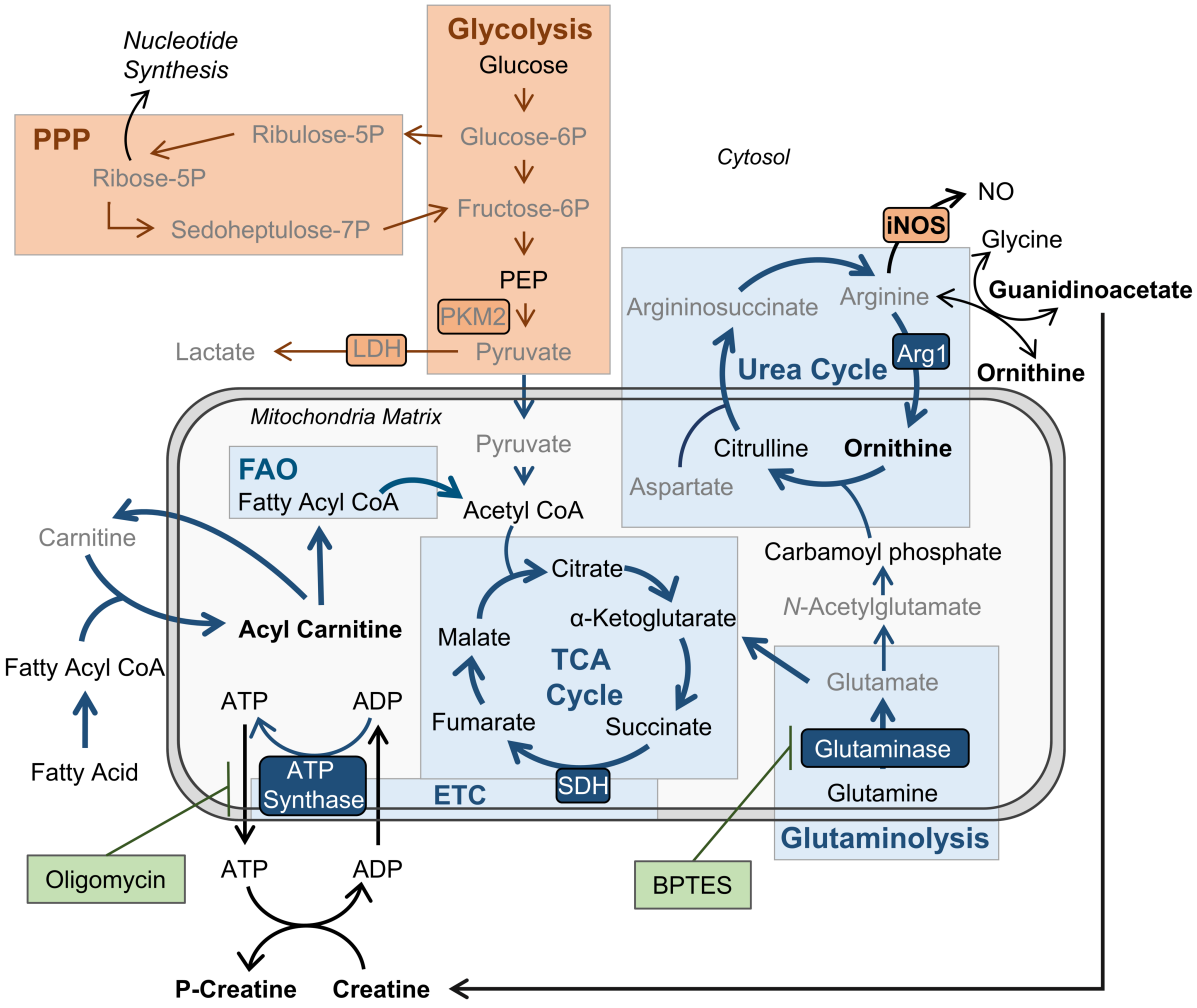

Figure 5. BMDMs trained with IL-4 and IL-13 retain M2-typical metabolism: schematic summary of results.

Pathways have been simplified. Key: metabolic pathways strongly upregulated by M1/M2 macrophage activation are highlighted by red/blue colored boxes, respectively. Inhibitors are indicated by green boxes. Arrow width represents which pathways are implicated (thicker) or not (narrower) in trained M(4/13) following stimulation with irradiated *M. tuberculosis* (Mtb). Metabolites (measured by LC-MS) or enzymes (measured by qPCR) written in bold or in grey text are enhanced or reduced respectively compared with untrained macrophages. Trained M(4/13) do not employ classical activated macrophage metabolism – aerobic glycolysis and pentose phosphate pathway (PPP) – and instead employ alternative activated macrophage metabolism, characterized by production of ATP through the tricarboxylic acid (TCA) cycle, coupled with the electron transport chain (ETC) via oxidative phosphorylation (OXPHOS), as well as enhanced use of the urea cycle. Glutaminolysis, FAO and ATP synthesis regulation are implicated. This is demonstrated by inhibitor experiments and by changed expression of metabolites. Abbreviations: LDH, lactate dehydrogenase; NO, nitric oxide; P, phosphate; PEP, Phosphoenolpyruvic acid; PKM2, pyruvate kinase M2; SDH, succinate dehydrogenase.

IL-10 Negatively Regulates IL-4 and IL-13 Induced Training

A key consideration regarding alternative macrophage activation and TB infection is the influence of concurrent parasitic disease. Along with IL-4 and IL-13, parasites can induce production of the regulatory cytokine IL-10 (Gause, Wynn, & Allen, 2013; Roy et al., 2018), which moreover promotes

alternative macrophage activation (Bystrom et al., 2008; Mantovani et al., 2004). Furthermore, it has been shown that products of the helminth *F. hepatica* can train macrophages to secrete more IL-10 following secondary LPS stimulation (Quinn et al., 2019). Given its association with alternative macrophage activation and parasitic infection, we next considered the potential role of IL-10 in IL-4 induced macrophage innate memory responses.

BMDMs were activated with IL-4, IL-13 and IL-10 (M(4/13/10)) to compare how this phenotype may have differed from M(4/13). Following acute activation, M(4/13/10) had similarly elevated levels of *Arg1* as M(4/13) and a comparably minor induction of *Nos2* (**Figure 6A**). The addition of IL-10 moreover caused even greater augmentation of M2-associated *Chil3* and *Retnla* expression. Accompanying flow cytometry analysis demonstrated that both M(4/13/10) and M(4/13) exhibited reduced expression of CD80, compared with M(-), along with enhanced expression of CD206, where the M(4/13/10) had greater CD206 expression (**Figure S6A**). Regarding MHC II, only M(4/13) displayed enhanced expression compared with M(-). The similar upregulation of M2-characteristic markers indicated that M(4/13) and M(4/13/10) were two types of alternatively activated macrophages.

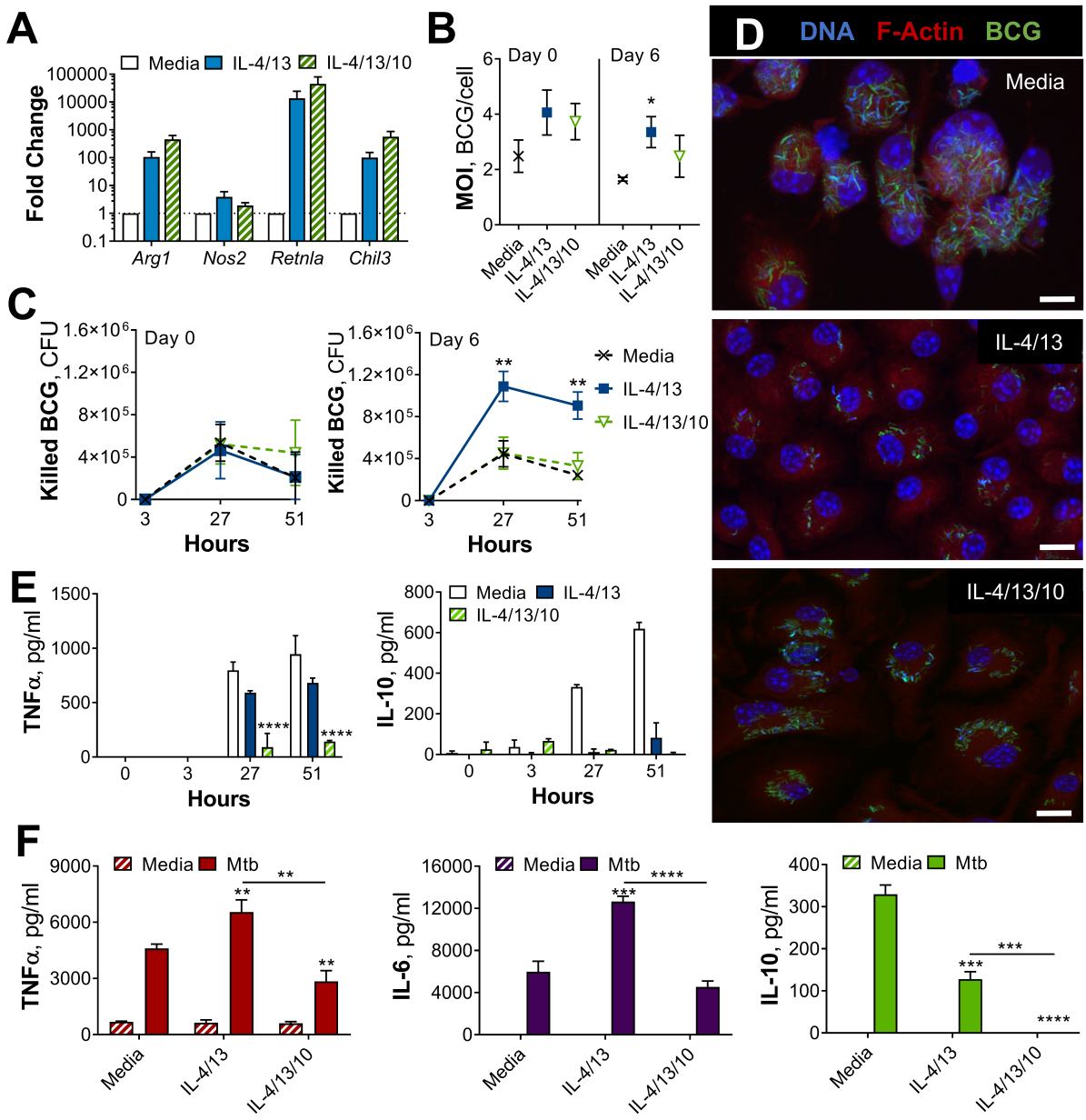

Figure 6. IL-10 inhibits bactericidal and pro-inflammatory training induced by IL-4 and IL-13.

(**A**) qPCR of indicated mRNA in BMDMs following 24 h incubation with media or IL-4 and IL-13, with or without IL-10, standardized to media control (n=4). Mean ± SD are shown. (**B-E**) BCG Denmark MOI (B) killing after h as indicated (C) as measured by CFU per 0.5 × 10^6 BMDMs on Day 0 or Day 6. Representative images of Hoechst- (blue), modified auramine-O- (green) and phalloidin (red)-stained BMDMs were taken on Day 6, 27 h after BCG incubation (D). Cytokine secretion on Day 6, at h indicated (E). BMDMs were previously incubated with media or IL-4 and IL-13, with or without IL-10, for 24 h on Day -1. (B-C, E) representative results (n = 2) are shown as mean ± SD (B, E) or SEM (C) and analyzed by student's t-test compared with media (B) or multiple t-tests, with Holm-Sidak correction, comparing with or without IL-10 (C, E). (**F**) Cytokine secretion following BMDM incubation with media or IL-4 and IL-13, with or without IL-10, for 24 h on Day -1 and incubated for 24 h with media or irradiated *M. tuberculosis* (Mtb) on Day 6. Mean ± SD (n = 3) are shown and analyzed by student's t-test. * $p \leq 0.05$, ** $p \leq 0.01$, **** $p \leq 0.0001$.

A similar comparison was made at Day 7, where both M(4/13) and M(4/13/10) retained enhanced *Arg1*, *Retnla* and *Chil3* expression and displayed enhanced *Nos2* expression compared with naïve M(-) (**Figure S6B**). Regarding accompanying CD80, CD206 and MHC II expression (**Figure S6C**): in all tested conditions, CD206 expression was comparable between M(4/13) and M(4/13/10), whereas CD80 expression was elevated in M(4/13/10). Furthermore, M(4/13) retained an elevated expression of MHC II, which increased two- and four-fold following stimulation with Mtb and PAM3CSK4, respectively, whereas this elevation did not occur to the same degree in M(4/13/10).

Our next question was how the addition of IL-10 during alternative activation would affect mycobacterial killing capacity. The BMDMs were incubated with roughly 30 BCG per cell on Day 0 or Day 6. There were some differences in bacterial uptake, where M(4/13) took up more bacteria per cell on Day 6, leading to an MOI of 1-4 (**Figure 6B**). CFU counts (**Figure S1C**) were used to calculate killing of internalized BCG. On Day 0, M(-), M(4/13) and M(4/13/10) displayed comparable killing capacity (**Figure 6C**). Moreover, BCG infection did not induce detectable levels of TNFα or IL-10 (**Figure S1D**). On Day 6, M(-) and M(4/13/10) maintained a similar level of BCG killing, whereas M(4/13) displayed enhanced bactericidal capacity. This indicated that IL-10 hindered the enhanced bactericidal response induced by prior IL-4 and IL-13 macrophage activation. The difference in bacterial killing capacity was further supported by confocal microscopy 27 hours after infection, where it was observed that M(-) and M(4/13/10) had markedly more bacteria per cell compared with M(4/13) (**Figure 6D**). Furthermore, whereas M(4/13) showed a shift towards pro-inflammatory cytokine secretion, with IL-10 secretion being reduced whilst TNFα production was largely intact, M(4/13/10) secreted significantly less TNFα than M(4/13), whilst IL-10 secretion was not enhanced (**Figure 6E**). This would indicate that IL-10 regulated the training induced by IL-4 and IL-13, preventing both the enhancement of killing capacity and the accompanying pro-inflammatory cytokine profile.

This difference in cytokine response profile was confirmed by carrying out similar experiments with Mtb. Whilst M(4/13), secreted lower concentrations of TNFα, IL-6 and IL-10 than M(-) on Day 1 (**Figure S6D**), but elevated TNFα and IL-6 by Day 7 (**Figure 6F**), while inflammatory cytokine secretion by M(4/13/10) was reduced on both Day 1 and Day 7. Furthermore, whilst both M(4/13) and M(4/13/10) displayed similar expression of *Arg1* following Mtb stimulation on Day 7, the addition of IL-10 during activation hindered the upregulation of *Nos2* observed in trained M(4/13) (**Figure S6E**). Overall, IL-10 appeared to impede the enhanced pro-inflammatory and bactericidal capacity induced by IL-4 and IL-13 innate training.

Discussion

Although "classical" and "alternative" activation are used to describe the two extremes of macrophage polarization, the reality is a broad spectrum of activation states, affected by a multitude of signals. Moreover, growing evidence has shown that the macrophage population during *M. tuberculosis* infection is highly heterogeneous, and thus elucidating which subtypes best contain the bacterium is critical for understanding disease control (A. Khan, Singh, Hunter, & Jagannath, 2019). Alternative macrophage activation is moreover relevant to TB pathology, both because alveolar macrophages – the initial hosts of *M. tuberculosis* upon infection – are biased towards alternative activation (Huang, Nazarova, & Russell, 2019), and also considering the influence of concurrent parasitic infection. The current study shows that alternative macrophage activation stimuli impact innate immune memory at least in part via epigenetic modification (**Figure S3C**); an additional dimension to the noted diversity among macrophage populations.

Whilst acute alternative macrophage activation has been demonstrated to lead to reduced control of *M. tuberculosis* growth (Kahnert et al., 2006), resulting in greater bacterial burden (Moreira-Teixeira et al., 2016; Orecchioni et al., 2019), there have been some conflicting data concerning the interplay between parasites and mycobacterial infections. Parasitic infection has been shown to enhance mycobacterial bacterial burden *in vivo* (Monin et al., 2015; Potian et al., 2011) and enhance human TB pathology (Amelio et al., 2017; Mabbott, 2018), but has in some cases also been shown to enhance protection against mycobacterial infection (Aira, Andersson, Singh, McKay, & Blomgran, 2017; O'Shea et al., 2018). Furthermore, discrepancies have been highlighted specifically regarding macrophage activation. In a model of *M. tuberculosis* macrophage infection *in vitro*, prior incubation (48hr) with antigens from *Hymenolepis diminuta*, *Trichuris muris* and *Schistosoma mansoni* resulted in alternative macrophage activation, but only incubation with the *H. diminuta* and *T. muris* antigens resulted in enhanced mycobacterial growth (Aira et al., 2017). Moreover, the increased growth was accompanied by enhanced secretion of IL-10. This however was not surprising, given that IL-10 has been demonstrated to prevent phagolysosome maturation in human macrophages (O'Leary et al., 2011) and promote TB disease progression in mice (Beamer et al., 2008). Herein, an additional mechanism is proposed, as IL-10 appears to be a key determinant of alternative macrophage training and subsequent control of mycobacterial challenge. BMDM activation with IL-4 and IL-13, with or without the addition of IL-10, resulted in similar activation states: comparable expression of *Arg1*, *Retnla* and *Chil3* on Day 0 (**Figure 6A**) and 7 (**Figure S6B**), reduced expression of CD80 and upregulation of CD206 on Day 0 (**Figure S6A**), as well as reduced secretion of cytokines TNFα, IL-6 and IL-10 following stimulation with Mtb on Day 0 (**Figure S6D**). Whilst this hyporesponsive profile was maintained in the M(4/13/10), the trained M(4/13) on the other hand demonstrate enhanced pro-

inflammatory and bactericidal mechanisms in response to mycobacterial challenge a week after initial activation (**Figure 6**). This intimated that IL-10 was a negative regulator of innate training induced by IL-4 and IL-13 and supports that distinct cytokine mediated modes of alternative macrophage activation differ regarding their innate memory programming.

The trained M(4/13) in response to mycobacterial challenge adopted a phenotype similar to classically activated BMDMs: a skewing towards pro-inflammatory cytokine secretion with concomitant increased expression of *Nos2* and NO production (**Figure 2**), as well as enhanced mycobacterial killing capacity (**Figure 1**). Classical macrophage activation is intrinsically linked with a glycolytic shift in metabolism; it is thus not surprising that prior work has identified an enhancement of glycolysis as critical for efficient *M. tuberculosis* killing (Gleeson et al., 2016; Huang et al., 2018) and that impeding glycolysis attenuates macrophages ability to control TB infection (Hackett et al., 2020). Moreover, upon *M. tuberculosis* infection, macrophages appear to undergo a biphasic metabolic profile, where they switch from an initial increase in glycolytic metabolism to an enhancement of the TCA cycle and OXPHOS; a switch which allows mycobacterial survival and disease progression (Shi et al., 2019). As such, it was expected that the trained M(4/13) would shift towards glycolytic metabolism. However, this was not the case, as Mtb stimulation resulted in enhanced OCR and SRC, indicating the use and upregulation of OXPHOS (**Figure 3**). Furthermore, LC-MS analysis of metabolites indicated increased use of FAO, as well as enhanced creatine, further supporting the continued use of M2-typical metabolism. This was moreover confirmed with the use of the ATP synthase inhibitor oligomycin, where it was demonstrated that inhibition of OXPHOS reduced trained M(4/13) cytokine secretion, whereas by contrast M(IFNγ/LPS) TNFα upregulation was unaffected. Furthermore, when trained M(4/13) were incubated in a glucose depleted environment during the week preceding secondary stimulation, the glucose depletion enhanced the pro-inflammatory shift: increased TNFα and IL-6 secretion combined with reduced IL-10 production (**Figure 4B**). This was a stark contrast to the effect of glucose depletion on untrained M(-) and trained M(IFNγ/LPS), where the secretion of all measured cytokines was attenuated. This contrast between M(4/13) and M(IFNγ/LPS) cemented their differences regarding metabolic dependency on glucose.

It is of note that the addition of a glycolysis inhibitor reduced cytokine secretion, from M(-), M(IFNγ/LPS), as well as M(4/13) following secondary stimulation (**Figures S5A-B**). That inhibition of glycolysis impeded pro-inflammatory cytokine secretion, but glucose depletion did not, indicated that glycolysis in trained M(4/13) was fueling the TCA cycle and downstream OXPHOS, and upon glucose depletion other pathways, such as glutaminolysis, were compensating for this loss. Glutaminolysis has been shown to be upregulated following macrophage activation with IL-4 and has been demonstrated to compensate for glycolysis inhibition in driving the TCA cycle and OXPHOS (Wang et al., 2018). In the

present study, it was moreover observed that the use of a glutaminolysis inhibitor reduced TNFα and IL-6 secretion following secondary stimulation in trained M(4/13) specifically, and not in untrained M(-) or M(IFNγ/LPS) (**Figure 4A**). It should be noted that prior work has identified differences in macrophage metabolic profiles in response to infection with live *M. tuberculosis* compared with the killed bacterium or infection with attenuated BCG (Cumming, Addicott, Adamson, & Steyn, 2018). However, the consensus is that classic macrophage activation, and an accompanying shift to glycolytic metabolism, is paramount for effective mycobacterial killing and propagation of inflammatory responses. It is surprising therefore that these results summarily intimated that trained M(4/13) maintain OXPHOS to fuel anti-mycobacterial responses.

The metabolic profile in trained M(4/13), as summarized in **Figure 5**, is not only distinct from classically activated macrophages, but also from that seen with other training stimuli, such as β-glucan. Innate training is being tested as a means to bolster innate immunity against *M. tuberculosis* (Khader et al., 2019) and it was recently reported that training with β-glucan was protective against subsequent *M tuberculosis* infection, as seen by enhanced human monocyte pro-inflammatory cytokine secretion and increased mouse survival *in vivo* (Moorlag et al., 2020). Similar to classical macrophage activation, β-glucan training results in a glycolytic shift, as demonstrated in human monocytes (Cheng et al., 2014). As such, the phenotype of the trained M(4/13) is distinct from other macrophage phenotypes previously demonstrated to protect against TB, and thus offers an additional avenue for future research regarding strategies for combatting this disease.

Van den Bossche et al. in 2016 highlighted a key adaptive distinction between classical and alternative macrophage activation: that alternatively activated macrophages can be “re-polarized” due to their metabolic versatility, whereas the mitochondrial dysfunction which occurs during classical macrophage activation prevents such reprogramming (Van den Bossche et al., 2016). In the current study, an additional adaptive capacity is identified: that activation with IL-4 and IL-13 programs BMDMs to better respond to a mycobacterial challenge, whilst crucially retaining their metabolic diversity.

In conclusion, our work presents mechanistic insight into how innate training via IL-4 and IL-13 can enhance macrophage pro-inflammatory responses and mycobacterial killing. This unexpected finding shows how macrophage plasticity belies the usual M1-M2 dichotomy and provides a new framework to explore the impact of comorbidities, such as parasitic infections, on TB disease burden.

573 ## Materials and Methods

574 ### Table 1. Sources of materials and resources

REAGENT or RESOURCE	SOURCE	IDENTIFIER
Antibodies		
Anti-CD11b-APC-eFluor 780	Thermo Fisher Scientific, Waltham, Massachusetts	Cat# 47-0112-82, RRID: AB_1603193, Clone M1/70
Anti-CD206-PE	BioLegend, San Diego, California	Cat# 141706, RRID: AB_10895754, Clone C068C2
Anti-CD80-FITC	BD Biosciences, Franklin Lakes, New Jersey	Cat# 561954, RRID: AB_10896321, Clone 16-10A1
Anti-F4/80-PerCP-Cy5.5	Thermo Fisher Scientific, Waltham, Massachusetts	Cat# 45-4801-82, RRID: AB_914345, Clone BM8
Anti-MHC class II-eFlour 450	Thermo Fisher Scientific, Waltham, Massachusetts	Cat# 48-5321-82, RRID: AB_1272204, Clone M5/114.15.2
Fc block: Anti-CD16/CD32	BD Biosciences, Franklin Lakes, New Jersey	Cat# 553142, RRID: AB_394657, Clone 2.4G2
Bacterial and virus strains		
Non-viable irradiated *Mycobacterium tuberculosis* strain H37Rv	BEI resources, Manassas, Virginia	NR-49098
Bacille Calmette-Guérin (BCG) Denmark 1331	Gift to Prof. Gordon from Prof. Behr, McGill University, Canada	N/A
Chemicals, peptides, and recombinant proteins		
2-deoxyglucose, 2-DG	Sigma Aldrich, Burlington, Massachusetts	Cat# D8375
4% PFA in PBS	Santa Cruz Biotechnology, Dallas, Texas	Cat# NC0238527
Acetonitrile	Thermo Fisher Scientific, Waltham, Massachusetts	Cat# 10001334
Antimycin-A	Sigma Aldrich, Burlington, Massachusetts	Cat# A8674

BPTES	Sigma Aldrich, Burlington, Massachusetts	Cat# SML0601-5mg
CpG	InvivoGen, San Diego, California	Cat# ODN M362
DMEM (high glucose)	Sigma Aldrich, Burlington, Massachusetts	Cat# D5671
DMEM (no glucose)	Gibco, Waltham, Massachusetts	Cat# 11966025
dNTP Mix	Meridian Bioscience, Cincinnati, Ohio	Cat# BIO-39028
FBS	Biosera, Kansas City, Missouri	Batch# 015BS551
FCCP	Sigma Aldrich, Burlington, Massachusetts	Cat# C2920
Fixable Viability Stain 510	Invitrogen, Waltham, Massachusetts	Cat# 564406
Glucose	Sigma Aldrich, Burlington, Massachusetts	Cat# G8270
L-Glutamine	Gibco, Waltham, Massachusetts	Cat# 25030-024
Glycerol	Sigma Aldrich, Burlington, Massachusetts	Cat# G2025
Heat-Shocked Bovine Serum Albumin (BSA)	Thermo Fisher Scientific, Waltham, Massachusetts	Cat# 12881630
Hoechst 33342	Thermo Fisher Scientific, Waltham, Massachusetts	Cat# 10150888
KAPA SYBR® FAST Rox low qPCR Kit Master Mix	Sigma Aldrich, Burlington, Massachusetts	Cat# KK4622
LPS, *Escherichia coli*, serotype R515	Enzo, Farmingdale, New York	Cat# ALX-581-007-L002
Methanol	Thermo Fisher Scientific, Waltham, Massachusetts	Cat# 10284580
Middlebrook 7H11 powder	Sigma Aldrich, Burlington, Massachusetts	Cat# M0428

Middlebrook 7H9 powder	Sigma Aldrich, Burlington, Massachusetts	Cat# M0178
M-MLV reverse transcriptase	Promega, Madison, Wisconsin	Cat# M3683
Modified Auramine-O stain and quencher	Scientific Device Laboratory, Des Plaines, Illinois	Cat# 345-04L
MTA	Sigma Aldrich, Burlington, Massachusetts	Cat# D5011-25MG
Oligomycin	Sigma Aldrich, Burlington, Massachusetts	Cat# 75351
PAM3CSK4	InvivoGen, San Diego, California	Cat# tlrl-pms
PBS, sterile	Gibco, Waltham, Massachusetts	Cat# 14190094
Penicillin-Streptomycin	Gibco, Waltham, Massachusetts	Cat# 15-070-063
Phalloidin-Alexa Fluor 647	Invitrogen, Waltham, Massachusetts	Cat# A22287
Poly I:C	InvivoGen, San Diego, California	Cat# tlrl-pic
Pyruvate	Sigma Aldrich, Burlington, Massachusetts	Cat# P5280
Radio-Immunoprecipitation Assay (RIPA) buffer	Sigma Aldrich, Burlington, Massachusetts	Cat# R0278-50ML
Random Hexamer Primer Mix	Meridian Bioscience, Cincinnati, Ohio	Cat# BIO-38028
Recombinant murine IFNγ	Peprotech, Cranbury, New Jersey	Cat# 315-05
Recombinant murine IL-10	Peprotech, Cranbury, New Jersey	Cat# 210-10
Recombinant murine IL-13	Peprotech, Cranbury, New Jersey	Cat# 210-13
Recombinant murine IL-4	Peprotech, Cranbury, New Jersey	Cat# 214-14
Resiquimod/R848	InvivoGen, San Diego, California	Cat# tlrl-r848
Reverse Transcriptase Buffer	Promega, Madison, Wisconsin	Cat# A3561

RNAseOUT	Invitrogen, Waltham, Massachusetts	Cat# 10777019
Rotenone	Sigma Aldrich, Burlington, Massachusetts	Cat# R8875
Seahorse Calibration Fluid pH 7.4	Agilent, Santa Clara, California	Part# 100840-000
Seahorse XF DMEM Medium	Agilent, Santa Clara, California	Cat# 103575-100
Sodium Chloride	Sigma Aldrich, Burlington, Massachusetts	Cat# S9888
Tween20	Sigma Aldrich, Burlington, Massachusetts	Cat# P1379-1L
Valine-d8	CK isotopes, Newtown Unthank, UK	Cat# DLM-488
Vectashield mounting media	VWR, Vector Laboratories	Cat# 101098-042
Water, sterile	Baxter, Deerfield, Illinois	Cat# UKF7114
Critical commercial assays		
BCA Protein Assay Kit (Pierce™)	Thermo Fisher Scientific, Waltham, Massachusetts	Cat# 23225
Griess Reagent System kit	Promega, Madison, Wisconsin	Cat# G2930
High Pure RNA Isolation Kit	Roche, Basel, Switzerland	Cat# 11828665001
Mouse IL-10 ELISA MAX	BioLegend, San Diego, California	Cat# 431411
Mouse IL-6 ELISA MAX	BioLegend, San Diego, California	Cat# 431301
Mouse TNFα DuoSet ELISA	R&D Systems, Minneapolis, Minnesota	Cat# DY410
Deposited data		
Raw and analyzed data	This Paper	DOI: 10.17632/ncbph43m85.1.
Experimental models: Cell lines		

L929	gift of Dr. Muñoz-Wolf, Trinity College, Dublin	N/A
Experimental models: Organisms/strains		
WT mice used for cell isolations	In-house colonies	C57BL/6JOlaHsd
Oligonucleotides		
Primers for *Actb*	See Table S1	N/A
Primers for *Arg1*	See Table S1	N/A
Primers for *Chitl3*	See Table S1	N/A
Primers for *Ldha*	See Table S1	N/A
Primers for *Myc*	See Table S1	N/A
Primers for *Nos2*	See Table S1	N/A
Primers for *Pkm2*	See Table S1	N/A
Primers for *Retnla*	See Table S1	N/A
Primers for *Sdha*	See Table S1	N/A
Primers for *Tbp*	See Table S1	N/A
Software and algorithms		
FlowJo 7	FlowJo LLC, Franklin Lakes, New Jersey	https://www.flowjo.com/solutions/flowjo
MetaboAnalyst 5.0	Xia Lab @ McGill	https://www.metaboanalyst.ca/
Microsoft Office Excel	Microsoft, Redmond, Washington	https://products.office.com/en-au/excel
Prism 8.2	GraphPad Software, San Diego, California	https://www.graphpad.com/scientific-software/prism/
Tracefinder 5.0	Thermo Fisher Scientific, Waltham, Massachusetts	https://www.thermofisher.com/ie/en/home/industrial/mass-spectrometry/liquid-chromatography-mass-spectrometry-lc-ms/lc-ms-software/lc-ms-data-acquisition-software/tracefinder-software.html

575

Experimental Model and Subject Details

Animals

Mice used for primary cell isolation were eight to 16-week-old wild-type C57BL/6 mice that were bred in the Trinity Biomedical Sciences Institute Bioresources Unit. Animals were maintained according to the regulations of the Health Products Regulatory Authority (HPRA). Animal studies were approved by the TCD Animal Research Ethics Committee (Ethical Approval Number 091210) and were performed under the appropriate license (AE191364/P079).

Cell Isolation and Culture

Bone marrow-derived macrophages (BMDMs) were generated as described previously by our group.(Lebre, Hanlon, Boland, Coleman, & Lavelle, 2018) Briefly, bone marrow cells were extracted from the leg bones and were cultured in high glucose DMEM, supplemented with 8% v/v fetal bovine serum (FBS), 2 mM L-glutamine, 50 U ml^{-1} penicillin, 50 µg ml^{-1} streptomycin (hereafter referred to as complete DMEM [cDMEM]). Cells were plated on non-tissue cultured treated petri dishes (Corning) and supplemented with 25% v/v of L929 cell line conditioned medium containing macrophage colony-stimulating factor (M-CSF) on day -8. Fresh medium was added on day -5 and on day -2 adherent cells were detached by trypsinization and collected. Unless specified otherwise, for acute/polarization studies, BMDMs were seeded in 12-well plates at 0.9×10^6 BMDMs per well, and for training studies, BMDMs were seeded in 24-well plates at 0.2×10^6 BMDMs per well.

On day -1 BMDMs were cultured with medium (naïve/untrained) or activated with 25 ng ml^{-1} IFNγ with 10 ng ml^{-1} LPS (classical activation), or 40 ng ml^{-1} IL-4 with 20 ng ml^{-1} IL-13, with or without 40 ng ml^{-1} IL-10 (alternative activation) – all included 15% L929 conditioned media. After 24 hours, the supernatant was replaced with fresh media (with 10% L929 conditioned media). For acute activation/polarization studies, the BMDMs were left to rest for 2 hours before experiment. For training studies, the BMDMs were left to rest, fed on day 3 (media supplemented with 7% L929 conditioned media) and experiments were carried out on day 6. The amount of L929 conditioned media added on each day was consistent for all experiments.

BCG Infection

Mature BMDMs were seeded in 24-well plates at 0.5×10^6 cells (acute activation) or 0.2×10^6 cells (training) per well on day -2. For imaging of internalized BCG in untrained and trained BMDMs, 0.2×10^6 BMDMs were seeded on circular glass coverslips (placed in 24 well plates, one coverslip per well) that had been previously treated with sodium hydroxide to aid attachment.

BMDMs were incubated with media (naïve) or activated as outlined above on day -1, for 24 hours before BMDMs were washed and fresh media was added. For acute activation studies, BMDMs

were infected with BCG Denmark minimum 3 hours later. For training studies, BMDMs were fed on day 3 and infected with BCG Denmark on Day 6.

Regarding infection dose (BCG per cell), for infection in acutely activated BMDMs, cell number per well was assumed to be 0.5×10^6. For infecting trained BMDMs, three extra wells were prepared for all conditions and BMDMs were removed from these wells by trypsinization on day 5, pooled and counted in triplicate. Prepared BCG single cell suspension (see below) was diluted to reach an intended infection dose of 5 BCG per cell (as measured by OD_{600}, where 0.1 is estimated to be 10×10^6 bacteria ml^{-1}). Each infection dose was measured via CFU counts (see below) and was thus subsequently corrected to an actual infection dose of roughly 30 BCG per cell.

3 hours post infection the supernatant was removed and the infected BMDMs were washed twice with Dulbecco's Phosphate Buffered Saline (PBS) to remove extracellular bacteria, and fresh media was added.

To measure cytokine secretion at each time point (3-, 27- and 51 hours post infection), supernatant was collected and filtered (polyethersulfone [PES] 0.22 µm Luer lock syringe filter; Millex-GP) to remove BCG, prior to specific cytokines being measured by ELISA.

For CFU counts, at each time point the media was removed, wells were washed once with PBS before the BMDMs were lysed with 0.05% Tween20 in water. The cell lysate was diluted in pre-warmed (37 °C) 7H9 media, and 50 µl of dilutions 10^{-2}-10^{-6} were spread onto enriched 7H11 agar plates by dotting. Agar plates were incubated at 37 °C for 6 weeks and colonies were counted once a week from week 2 and on. CFU counts 3 hours gave the multiplicity of infection (MOI).

For imaging internalized BCG (wells containing glass coverslips), media was removed, BMDMs were washed with PBS and then fixed with 4% paraformaldehyde (in PBS) overnight. The paraformaldehyde was then removed and coverslips were stored in PBS.

Stimulation Experiments

Naïve (media control) or activated BMDMs were incubated with media or secondary stimuli on day 0 (acute activation/polarization) or day 6 (training). Secondary stimuli: 150 µg ml^{-1} gamma-irradiated whole cells of *Mycobacterium tuberculosis* strain H37Rv (concentration measured by OD_{600}, where 100 mg ml^{-1} was 0.32), 35 ng ml^{-1} PAM3CSK4, 25 ng ml^{-1} LPS, 5 µg ml^{-1} Poly I:C, 0.55 µg ml^{-1} R848, 10 µg ml^{-1} CpG.

For histone methylation inhibition: on day -2 BMDMs were incubated with MTA (final concentration 1 mM) one hour prior to media incubation or activation as outlined above.

For metabolic inhibition experiments: on day 6 BMDMs were pre-incubated with 1mM 2-DG for 3 hours, 2 µM oligomycin or 10 µM BPTES 1 hour prior to media incubation or secondary stimulation.

For glucose depletion training experiment: untrained or trained BMDMs were incubated with either the regular high glucose cDMEM or glucose depleted cDMEM, with DMEM devoid of glucose (Gibco), from day -2 until incubation with media or secondary stimulation on Day 6 (fed day 3 with the same media as given on day -2). Note, the glucose depleted cDMEM included 8% v/v FBS and the same amount of L929 conditioned media as outlined previously, both of which provided a source of glucose.

Seahorse

All real-time measurements of oxygen consumption rate (OCR) and extracellular acidification rate (ECAR) were measured by using Seahorse system: Seahorse XFe96 Analyzer (Agilent). The analysis used was a Mitochondrial Stress Test (using a standard Agilent Seahorse protocol).

On day -2, mature BMDMs were seeded in a 96-well Seahorse plate (Agilent): 100,000 cells per well for acute activation studies or 30,000 cells per well for training studies. BMDMs were activated on day -1 as outlined and analyzed on either day 0 (24 hours after activation) or day 6 (fed on day 3), with or without secondary stimulation on day 5 (training studies).

The day before analysis, a Seahorse Cartridge (Agilent) was incubated overnight at 37 °C (incubator devoid of CO_2). The following day, the sterile water was replaced with Calibration Fluid at pH 7.4 incubated as before for 90 minutes before the analysis.

An hour before the analysis, in the Seahorse plate regular cDMEM was replaced with Seahorse XF DMEM, supplemented with 10 mM glucose, 1 mM pyruvate and 2 mM L-glutamine. The BMDMs were then incubated for an hour at 37 °C (incubator devoid of CO_2).

15 minutes before the analysis, the cartridge was removed and reagents/inhibitors were added to their respective ports: oligomycin (port A, final concentration 10 µM), FCCP (port B, final concentration 10 µM), rotenone and antimycin-A (port C, final concentrations 5 µM each).

The analysis was carried out according to the manufacturer's instructions. Recorded values less than zero were disregarded.

For training experiments, protein concentration was used to standardize the OCR and ECAR measurements. Supernatant was removed, cells were washed once in PBS and 10 µl of RIPA buffer was added per well. After pipetting up and down and scraping, the buffer was collected and samples from the same condition were pooled. 20 µl of pooled solution was used to measure protein concentration, using the Pierce bicinchoninic acid (BCA) assay kit (Thermo Scientific) according to the manufacturer's instructions (microplate procedure). Absorbance was measured at 560 nm.

Metabolomics (LC-MS) sample preparation

On day -2, BMDMs were seeded in 6-well plates: 1×10^6 cells/well and activated on day -1 with IL-4/13 as outlined or incubated with media. BMDMs were fed on day 3 and incubated with irradiated *M. tuberculosis* on Day 6 for 24 hours. Prior to metabolite extraction, cells were counted using a separate counting plate prepared in parallel and treated exactly like the experimental plate. Supernatant was removed and cells were washed once in PBS. After aspiration, the BMDMs were kept at -80 °C or on dry ice. Metabolites were extracted by adding chilled extraction buffer (500 µl/1×10^6 cells), followed by scraping (carried out on dry ice). Buffer was transferred to chilled eppendorf tubes and shaken in a thermomixer at maximum speed (2000 rpm) for 15 minutes at 4 °C. Following centrifugation at maximum speed for 20 minutes, roughly 80% of supernatant was transferred into labelled LC-MS vials, taking care to avoid pellet and any solid debris.

Flow Cytometry

On day -2, 0.8×10^6 mature BMDMs were seeded on non-tissue cultured treated 35 mm petri dishes (Corning) and activated as previously outlined on Day -1. The naïve or activated/trained BMDMs were harvested at two separate time points: day 0 (24 hours post activation for acute activation characterisation) or day 6 (fed on day 3), with or without secondary stimulation on day 5 as specified in figure legends (training experiments).

For analysis, BMDMs were placed on ice for 30 min before harvesting with PBS-EDTA (5 mM) solution by gently pipetting up and down and transferring to flow cytometry tubes. Cells were incubated with Fixable Viability Stain 510 at RT for 15 min. After washing with PBS, cells were stained with anti-mouse Fc block, 15 minutes prior staining with CD80-FITC, CD206-PE, F4/80-PerCP-Cy5.5, CD11b-APC-eFluor 780, MHC class II-eFluor 450 for an additional 30 min at 4 °C. The cells were washed with PBS and resuspended in flow cytometry buffer (1% FBS in PBS). Samples were acquired on a BD Canto II flow cytometer and the data was analysed by using FlowJo software.

Method Details

BCG Preparation and Plating

Bacille Calmette-Guérin (BCG) Denmark (OD_{600} 0.1) was incubated in 7H9 media at 37 °C with rotation until the OD_{600} 0.5-0.8 (logarithmic growth phase) was reached.

Single cell suspension was prepared as follows: bacteria were pelleted by centrifugation and 7H9 media was removed. Bacteria were vortexed with glass beads before pre-warmed (37 °C) DMEM was added and bacteria were left to sediment for 5 minutes. Bacterial suspension was carefully collected (avoiding disruption of the pellet) and centrifuged again to pellet large clumps. Suspension

was collected (avoiding the pellet). Suspension was passed through a 26G needle 15 times to disaggregate bacterial clumps.

Bacterial concentration was estimated by OD_{600} (where 0.1 was estimated as 10×10^6 bacteria ml^{-1}) and infection dose was confirmed by colony forming unit (CFU) counts.

7H11 agar plates (for CFU counts) were made up as follows: 10.5 g middlebrook 7H11 powder and 2.5 ml glycerol was dissolved in distilled water to reach 500 ml and autoclaved. Once cooled sufficiently, 50 ml sterile-filtered (0.22 µm; SteriCup [Millipore]) albumin-dextrose-sodium chloride (ADN) enrichment was added. For 1 liter of ADN enrichment: 50 g fatty acid-free, heat-shocked bovine serum albumin, 8.5 g sodium chloride and 20 g glucose were dissolved in sterile water to reach 1 liter.

Staining and Imaging of Internalized BCG

For staining the coverslips contained in 24-well plates, PBS was removed and 17 µM Hoechst 33342 and 7.5 U Phalloidin-Alexa Fluor 647 (in 1 ml PBS) was added to each well. After half an hour (in the dark), the solution was removed and the coverslips were washed with PBS. 200 µl Modified Auramine-O stain was added for 2 minutes (in the dark), after which the stain was removed and the wells were washed with PBS. To quench any extracellular BCG, 200 µl Auramine-O Quencher de-colorizer was added for 2 minutes (in the dark) and then the quencher was removed and the coverslips were washed with PBS. The coverslips were then fixed onto glass slides: 2 µl Vectashield mounting media was used per coverslip and clear nail polish was applied around the edge and allowed to dry completely. The coverslips were stained and imaged the same day.

Images of all samples were obtained using a Leica SP8 confocal microscope, taken with x40 magnification oil objective. Z-stack images through the entire cell were obtained and representative images were taken from these stacks.

Liquid Chromatography coupled to Mass Spectrometry (LC-MS)

Extraction buffer for isolating metabolites: 50% LC-MS grade methanol, 30% LC-MS grade acetonitrile, 20% ultrapure water (internal filtration system), valine-d8 final concentration 5 µM.

Hydrophilic interaction chromatographic (HILIC) separation of metabolites was achieved using a Millipore Sequant ZIC-pHILIC analytical column (5 µm, 2.1 × 150 mm) equipped with a 2.1 × 20 mm guard column (both 5 mm particle size) with a binary solvent system. Solvent A was 20 mM ammonium carbonate, 0.05% ammonium hydroxide; Solvent B was acetonitrile. The column oven and autosampler tray were held at 40 °C and 4 °C, respectively. The chromatographic gradient was run at a flow rate of 0.200 mL/min as follows: 0–2 min: 80% B; 2-17 min: linear gradient from 80% B to 20% B; 17-17.1 min: linear gradient from 20% B to 80% B; 17.1-22.5 min: hold at 80% B. Samples were randomized and analysed with LC–MS in a blinded manner with an injection volume was 5 µl. Pooled

samples were generated from an equal mixture of all individual samples and analysed interspersed at regular intervals within sample sequence as a quality control.

Metabolites were measured with a Thermo Scientific Q Exactive Hybrid Quadrupole-Orbitrap Mass spectrometer (HRMS) coupled to a Dionex Ultimate 3000 UHPLC. The mass spectrometer was operated in full-scan, polarity-switching mode, with the spray voltage set to +4.5 kV/-3.5 kV, the heated capillary held at 320 °C, and the auxiliary gas heater held at 280 °C. The sheath gas flow was set to 25 units, the auxiliary gas flow was set to 15 units, and the sweep gas flow was set to 0 unit. HRMS data acquisition was performed in a range of *m/z* = 70–900, with the resolution set at 70,000, the AGC target at 1×10^6, and the maximum injection time (Max IT) at 120 ms. Metabolite identities were confirmed using two parameters: (1) precursor ion m/z was matched within 5 ppm of theoretical mass predicted by the chemical formula; (2) the retention time of metabolites was within 5% of the retention time of a purified standard run with the same chromatographic method. Chromatogram review and peak area integration were performed using the Thermo Fisher software Tracefinder 5.0 and the peak area for each detected metabolite was normalized against the total ion count (TIC) of that sample to correct any variations introduced from sample handling through instrument analysis. The normalized areas were used as variables for further statistical data analysis.

ELISA

For detection of secreted TNFα, IL-6 and IL-10 from BMDMs, supernatants were collected and cytokines quantified by ELISA according to manufacturers' instructions (R&D Systems or Biolegend), except antibody and sample volumes were halved.

Nitric oxide (NO) secretion

NO concentrations were quantified by indirect measurement of nitrite (NO_2^-) via the Griess Reagent System kit (Promega). The assay was carried out as per manufacturer's instructions and absorbance of 560 nm was measured.

Reverse Transcription Quantitative PCR (rt-qPCR)

RNA was isolated via High Pure RNA Isolation Kit (Roche) according to the manufacturer's instructions and RNA was eluted in 50 µl water. RNA (minimum 100 ng) was reverse transcribed into complementary DNA (cDNA) with an M-MLV reverse transcriptase, RNase H minus, point mutant, in reverse transcriptase buffer, mixed with dNTPs, random hexamer primers and ribonuclease inhibitor (RNAseOUT). Quantitative PCR was performed using KAPA SYBR® FAST Rox low qPCR Kit Master Mix in accordance with the instructions provided by the manufacturer, using QuantStudio 3 System technology. Primers (Table S1) were designed in Primer BLAST and/or were also checked in Primer

BLAST for specificity to the gene of interest. Where possible, primers were chosen to cross an exon-exon junction.

RNA expression was normalized to the internal references β-actin and/or TATAbox-binding protein, from the corresponding sample (Ct_{gene}–$Ct_{reference}$=ΔCt). Furthermore, ΔCt from control samples were subtracted from the ΔCt of each sample ($\Delta Ct_{treatment}$-ΔCt_{ctrl} =$\Delta\Delta Ct_{treatment}$). Fold change was calculated as $2^{(-\Delta\Delta Ct)}$. These calculations were carried out using Microsoft Excel.

Quantification and Statistical Analysis

Data were evaluated on either on Prism version 8 for Windows or via R for Metaboanalyst generated analysis. Differences between two independent groups were compared via unpaired Student's t-test. For BCG infection studies where two independent groups were compared at several time points, multiple t-test analysis was employed, with Holm-Sidak correction for multiple comparisons. Differences were considered significant at the values of * $P < 0.05$, ** $P < 0.01$, *** $P < 0.001$ and **** $P < 0.0001$.

Data and Code Availability

All data is available at Mendeley Data DOI: 10.17632/ncbph43m85.1.

Acknowledgements

The authors would like to thank Dr Gavin McManus for his assistance with the imaging studies.

M. Lundahl was funded by a Trinity College Dublin postgraduate studentship and this work is supported by Science Foundation Ireland (SFI) Research Centre, Advanced Materials and BioEngineering Research (AMBER) under Grant number 12/RC/2278_P2 E, SFI under Grant number 12/IA/1421 and 19FFP/6484 (E. Lavelle) and SFI under Grant number 15/CDA/3310 (E. Scanlan). S. Gordon and M. Mitermite acknowledge funding from Wellcome Trust PhD Studentship 109166/Z/15/A and SFI award 15/IA/3154.

Author Contributions

M.L.E.L. performed and analyzed all experiments and wrote the paper. M.M., B.S. and S.V.G provided assistance with BCG infection studies. D.G.R, N.C.W. and L.A.J.O. assisted with Seahorse experiments. M.Y. identified and quantified the metabolites via LC-MS and D.G.R and C.F. assisted with

metabolomics analysis. M.L.E.L., with the assistance of F.L. and A.L.G, developed the BMDM training protocol. M.L.E.L was supervised by E.M.S. and E.C.L. and the work was supervised by E.C.L.

Declaration of Interests

The authors declare no competing interests.

References

Abebe, F. (2012, September). Is interferon-gamma the right marker for bacille Calmette-Guérin-induced immune protection? The missing link in our understanding of tuberculosis immunology. *Clinical and Experimental Immunology*. Clin Exp Immunol. https://doi.org/10.1111/j.1365-2249.2012.04614.x

Aira, N., Andersson, A. M., Singh, S. K., McKay, D. M., & Blomgran, R. (2017). Species dependent impact of helminth-derived antigens on human macrophages infected with Mycobacterium tuberculosis: Direct effect on the innate anti-mycobacterial response. *PLoS Neglected Tropical Diseases*, *11*(2). https://doi.org/10.1371/journal.pntd.0005390

Amelio, P., Portevin, D., Reither, K., Mhimbira, F., Mpina, M., Tumbo, A., … Perreau, M. (2017). Mixed Th1 and Th2 Mycobacterium tuberculosis-specific CD4 T cell responses in patients with active pulmonary tuberculosis from Tanzania. *PLoS Neglected Tropical Diseases*, *11*(7). https://doi.org/10.1371/journal.pntd.0005817

Andersen, P., & Kaufmann, S. H. (2014). Novel vaccination strategies against tuberculosis. *Cold Spring Harb Perspect Med*, *4*(6). https://doi.org/10.1101/cshperspect.a018523

Arts, R. J. W., Moorlag, S. J. C. F. M., Novakovic, B., Li, Y., Wang, S. Y., Oosting, M., … Netea, M. G. (2018). BCG Vaccination Protects against Experimental Viral Infection in Humans through the Induction of Cytokines Associated with Trained Immunity. *Cell Host and Microbe*, *23*(1), 89-100.e5. https://doi.org/10.1016/j.chom.2017.12.010

Beamer, G. L., Flaherty, D. K., Assogba, B. D., Stromberg, P., Gonzalez-Juarrero, M., de Waal Malefyt, R., … Turner, J. (2008). Interleukin-10 Promotes Mycobacterium tuberculosis Disease Progression in CBA/J Mice . *The Journal of Immunology*, *181*(8), 5545–5550. https://doi.org/10.4049/jimmunol.181.8.5545

Bourigault, M. L., Segueni, N., Rose, S., Court, N., Vacher, R., Vasseur, V., … Quesniaux, V. F. J. (2013). Relative contribution of il-1α, il-1β and tnf to the host response to mycobacterium tuberculosis and attenuated m. Bovis bcg. *Immunity Inflammation and Disease*, *1*(1), 47–62. https://doi.org/10.1002/iid3.9

Brown, G. D., & Crocker, P. R. (2016). Lectin Receptors Expressed on Myeloid Cells. *Microbiology Spectrum*, *4*(5). https://doi.org/10.1128/microbiolspec.MCHD-0036-2016

Bystrom, J., Evans, I., Newson, J., Stables, M., Toor, I., van Rooijen, N., … Gilroy, D. W. (2008). Resolution-phase macrophages possess a unique inflammatory phenotype that is controlled by cAMP. *Blood*, *112*(10), 4117–4127. https://doi.org/10.1182/blood-2007-12-129767

Chatterjee, S., Talaat, K. R., van Seventer, E. E., Feng, C. G., Scott, A. L., Jedlicka, A., … Nutman, T. B. (2017). Mycobacteria induce TPL-2 mediated IL-10 in IL-4-generated alternatively activated macrophages. *PLoS ONE*, *12*(6). https://doi.org/10.1371/journal.pone.0179701

Cheng, S.-C., Quintin, J., Cramer, R. A., Shepardson, K. M., Saeed, S., Kumar, V., … Netea, M. G. (2014). mTOR- and HIF-1α-mediated aerobic glycolysis as metabolic basis for trained immunity. *Science (New York, N.Y.)*, *345*(6204), 1250684. https://doi.org/10.1126/science.1250684

Choreño-Parra, J. A., Weinstein, L. I., Yunis, E. J., Zúñiga, J., & Hernández-Pando, R. (2020, February 14). Thinking Outside the Box: Innate- and B Cell-Memory Responses as Novel Protective Mechanisms Against Tuberculosis. *Frontiers in Immunology*. Frontiers Media S.A. https://doi.org/10.3389/fimmu.2020.00226

Cohen, S. B., Gern, B. H., Delahaye, J. L., Adams, K. N., Plumlee, C. R., Winkler, J. K., … Urdahl, K. B. (2018). Alveolar Macrophages Provide an Early Mycobacterium tuberculosis Niche and Initiate Dissemination. *Cell Host & Microbe*, *24*(3), 439–446. https://doi.org/10.1016/j.chom.2018.08.001

Cumming, B. M., Addicott, K. W., Adamson, J. H., & Steyn, A. J. C. (2018). Mycobacterium tuberculosis induces decelerated bioenergetic metabolism in human macrophages. *ELife*, *7*. https://doi.org/10.7554/eLife.39169

Ferrante, C. J., & Leibovich, S. J. (2012). Regulation of Macrophage Polarization and Wound Healing. In *Adv Wound Care (New Rochelle)* (Vol. 1, pp. 10–16). Department of Cell Biology and Molecular Medicine and The Cardiovascular Research Institute, New Jersey Medical School, University of Medicine and Dentistry of New Jersey , Newark, New Jersey. https://doi.org/10.1089/wound.2011.0307

Flynn, J. L., Chan, J., Triebold, K. J., Dalton, D. K., Stewart, T. A., & Bloom, B. R. (1993). An essential role for interferon gamma in resistance to Mycobacterium tuberculosis infection. *J Exp Med*, *178*(6), 2249–2254.

Gabrilovich, D. I., Ostrand-Rosenberg, S., & Bronte, V. (2012). Coordinated regulation of myeloid cells by tumours. *Nature Reviews Immunology*, *12*(4), 253–268. https://doi.org/10.1038/nri3175

Gause, W. C., Wynn, T. A., & Allen, J. E. (2013, August 5). Type 2 immunity and wound healing: Evolutionary refinement of adaptive immunity by helminths. *Nature Reviews Immunology*. Nature Publishing Group. https://doi.org/10.1038/nri3476

Gleeson, L. E., Sheedy, F. J., Palsson-McDermott, E. M., Triglia, D., O'Leary, S. M., O'Sullivan, M. P., … Keane, J. (2016). Cutting Edge: Mycobacterium tuberculosis Induces Aerobic Glycolysis in Human Alveolar Macrophages That Is Required for Control of Intracellular Bacillary Replication . *The Journal of Immunology*, *196*(6), 2444–2449. https://doi.org/10.4049/jimmunol.1501612

Gordon, S., & Martinez, F. O. (2010). Alternative activation of macrophages: mechanism and functions. *Immunity*, *32*(5), 593–604. https://doi.org/10.1016/j.immuni.2010.05.007

Hackett, E. E., Charles-Messance, H., O'Leary, S. M., Gleeson, L. E., Muñoz-Wolf, N., Case, S., … Sheedy, F. J. (2020). Mycobacterium tuberculosis Limits Host Glycolysis and IL-1β by Restriction of PFK-M via MicroRNA-21. *Cell Reports*, *30*(1), 124-136.e4. https://doi.org/10.1016/j.celrep.2019.12.015

Huang, L., Nazarova, E. V., & Russell, D. G. (2019). Mycobacterium tuberculosis: Bacterial Fitness within the Host Macrophage. In *Bacteria and Intracellularity* (Vol. 7, pp. 127–138). American Society of Microbiology. https://doi.org/10.1128/microbiolspec.bai-0001-2019

Huang, L., Nazarova, E. V., Tan, S., Liu, Y., & Russell, D. G. (2018). Growth of Mycobacterium tuberculosis in vivo segregates with host macrophage metabolism and ontogeny. *Journal of Experimental Medicine*, *215*(4), 1135–1152. https://doi.org/10.1084/jem.20172020

Jouanguy, E., Lamhamedi-Cherradi, S., Lammas, D., Dorman, S. E., Fondanèche, M. C., Dupuis, S., … Casanova, J. L. (1999). A human IFNGR1 small deletion hotspot associated with dominant susceptibility to mycobacterial infection. *Nature Genetics*, *21*(4), 370–378. https://doi.org/10.1038/7701

892 Kahnert, A., Seiler, P., Stein, M., Bandermann, S., Hahnke, K., Mollenkopf, H., & Kaufmann, S. H. E.
893 (2006). Alternative activation deprives macrophages of a coordinated defense program to
894 Mycobacterium tuberculosis. *European Journal of Immunology*, *36*(3), 631–647.
895 https://doi.org/10.1002/eji.200535496

896 Keane, J., Gershon, S., Wise, R. P., Mirabile-Levens, E., Kasznica, J., Schwieterman, W. D., … Braun, M.
897 M. (2001). Tuberculosis Associated with Infliximab, a Tumor Necrosis Factor α–Neutralizing
898 Agent. *New England Journal of Medicine*, *345*(15), 1098–1104.
899 https://doi.org/10.1056/nejmoa011110

900 Khader, S. A., Divangahi, M., Hanekom, W., Hill, P. C., Maeurer, M., Makar, K. W., … Bill and Melinda
901 Gates Foundation Collaboration for TB Vaccine Discovery Innate Immunity Working Group18.
902 (2019). Targeting innate immunity for tuberculosis vaccination. *Journal of Clinical Investigation*,
903 *129*(9), 3482–3491. https://doi.org/10.1172/JCI128877

904 Khan, A., Singh, V. K., Hunter, R. L., & Jagannath, C. (2019, August 1). Macrophage heterogeneity and
905 plasticity in tuberculosis. *Journal of Leukocyte Biology*. John Wiley and Sons Inc.
906 https://doi.org/10.1002/JLB.MR0318-095RR

907 Khan, N., Downey, J., Sanz, J., Kaufmann, E., Blankenhaus, B., Pacis, A., … Divangahi, M. (2020). M.
908 tuberculosis Reprograms Hematopoietic Stem Cells to Limit Myelopoiesis and Impair Trained
909 Immunity. *Cell*, *183*(3), 752-770.e22. https://doi.org/10.1016/j.cell.2020.09.062

910 Kleinnijenhuis, J., Quintin, J., Preijers, F., Joosten, L. A. B., Ifrim, D. C., Saeed, S., … Netea, M. G. (2012).
911 Bacille Calmette-Guerin induces NOD2-dependent nonspecific protection from reinfection via
912 epigenetic reprogramming of monocytes. *Proceedings of the National Academy of Sciences of*
913 *the United States of America*, *109*(43), 17537–17542. https://doi.org/10.1073/pnas.1202870109

914 Lebre, F., Hanlon, D., Boland, J. B., Coleman, J., & Lavelle, E. C. (2018). Exfoliation in Endotoxin-Free
915 Albumin Generates Pristine Graphene with Reduced Inflammatory Properties. *Advanced*
916 *Biosystems*, *2*(12), 1800102 (1-15). https://doi.org/10.1002/adbi.201800102

917 Li, L., Ng, D. S. W., Mah, W. C., Almeida, F. F., Rahmat, S. A., Rao, V. K., … Lane, D. P. (2015). A unique
918 role for p53 in the regulation of M2 macrophage polarization. *Cell Death and Differentiation*,
919 *22*(7), 1081–1093. https://doi.org/10.1038/cdd.2014.212

920 Li, X. X., & Zhou, X. N. (2013). Co-infection of tuberculosis and parasitic diseases in humans: A
921 systematic review. *Parasites and Vectors*. Parasit Vectors. https://doi.org/10.1186/1756-3305-
922 6-79

923 Liu, L., Lu, Y., Martinez, J., Bi, Y., Lian, G., Wang, T., … Wang, R. (2016). Proinflammatory signal
924 suppresses proliferation and shifts macrophage metabolism from Myc-dependent to HIF1α-
925 dependent. *Proceedings of the National Academy of Sciences of the United States of America*,
926 *113*(6), 1564–1569. https://doi.org/10.1073/pnas.1518000113

927 Luiz, J. P. M., Toller-Kawahisa, J. E., Viacava, P. R., Nascimento, D. C., Pereira, P. T., Saraiva, A. L., …
928 Alves-Filho, J. C. (2020). MEK5/ERK5 signaling mediates IL-4-induced M2 macrophage
929 differentiation through regulation of c-Myc expression. *Journal of Leukocyte Biology*, *108*(4),
930 1215–1223. https://doi.org/10.1002/JLB.1MA0520-016R

931 Lundahl, M. L. E., Scanlan, E. M., & Lavelle, E. C. (2017). Therapeutic potential of carbohydrates as
932 regulators of macrophage activation. *Biochemical Pharmacology*, *146*, 23–41.
933 https://doi.org/10.1016/j.bcp.2017.09.003

934 Lundahl, M., Lynch, D. M., Barnes, D., McSweeney, L., Gorman, A., Lebre, F., … Scanlan, E. M. (2020).
935 Mycobacterial para-Hydroxybenzoic Acid-Derivatives (pHBADs) and Related Structures Induce
936 Macrophage Innate Memory. *ACS Chemical Biology*, *15*(9), 2415–2421.
937 https://doi.org/10.1021/acschembio.0c00378

938 Mabbott, N. A. (2018). The Influence of Parasite Infections on Host Immunity to Co-infection With
939 Other Pathogens. *Frontiers in Immunology*. NLM (Medline).
940 https://doi.org/10.3389/fimmu.2018.02579

941 Mantovani, A., Sica, A., Sozzani, S., Allavena, P., Vecchi, A., & Locati, M. (2004). The chemokine system
942 in diverse forms of macrophage activation and polarization. *Trends Immunol*, *25*(12), 677–686.
943 https://doi.org/10.1016/j.it.2004.09.015

944 Monin, L., Griffiths, K. L., Lam, W. Y., Gopal, R., Kang, D. D., Ahmed, M., … Khader, S. A. (2015).
945 Helminth-induced arginase-1 exacerbates lung inflammation and disease severity in
946 tuberculosis. *Journal of Clinical Investigation*, *125*(12), 4699–4713.
947 https://doi.org/10.1172/JCI77378

948 Moorlag, S. J. C. F. M., Khan, N., Novakovic, B., Kaufmann, E., Jansen, T., van Crevel, R., … Netea, M. G.
949 (2020). β-Glucan Induces Protective Trained Immunity against Mycobacterium tuberculosis
950 Infection: A Key Role for IL-1. *Cell Reports*, *31*(7). https://doi.org/10.1016/j.celrep.2020.107634

951 Moreira-Teixeira, L., Sousa, J., McNab, F. W., Torrado, E., Cardoso, F., Machado, H., … Saraiva, M.
952 (2016). Type I IFN Inhibits Alternative Macrophage Activation during Mycobacterium
953 tuberculosis Infection and Leads to Enhanced Protection in the Absence of IFN-γ Signaling.
954 *Journal of Immunology (Baltimore, Md. : 1950)*, *197*(12), 4714–4726.
955 https://doi.org/10.4049/jimmunol.1600584

956 Murray, P. J., & Wynn, T. A. (2011). Protective and pathogenic functions of macrophage subsets.
957 *Nature Reviews Immunology*, *11*(11), 723–737. https://doi.org/10.1038/nri3073

958 O'Leary, S., O'Sullivan, M. P., & Keane, J. (2011). IL-10 blocks phagosome maturation in mycobacterium
959 tuberculosis-infected human macrophages. *Am J Respir Cell Mol Biol*, *45*(1), 172–180.
960 https://doi.org/10.1165/rcmb.2010-0319OC

961 O'Neill, L. A. J., Kishton, R. J., & Rathmell, J. (2016). A guide to immunometabolism for immunologists.
962 *Nature Reviews Immunology 2016 16:9*, *16*(9), 553–565. https://doi.org/10.1038/NRI.2016.70

963 O'Shea, M. K., Fletcher, T. E., Muller, J., Tanner, R., Matsumiya, M., Bailey, J. W., … McShane, H. (2018).
964 Human Hookworm Infection Enhances Mycobacterial Growth Inhibition and Associates With
965 Reduced Risk of Tuberculosis Infection. *Frontiers in Immunology*, *9*, 2893.
966 https://doi.org/10.3389/fimmu.2018.02893

967 Orecchioni, M., Ghosheh, Y., Pramod, A. B., & Ley, K. (2019). Macrophage Polarization: Different Gene
968 Signatures in M1(LPS+) vs. Classically and M2(LPS–) vs. Alternatively Activated Macrophages.
969 *Frontiers in Immunology*, *10*, 1084 (1-14). https://doi.org/10.3389/fimmu.2019.01084

970 Ottenhoff, T. H. M., Doherty, T. M., Van Dissel, J. T., Bang, P., Lingnau, K., Kromann, I., & Andersen, P.
971 (2010, December). First in humans: A new molecularly defined vaccine shows excellent safety
972 and strong induction of long-lived Mycobacterium tuberculosis-specific Th1-cell like responses.
973 *Human Vaccines*. Hum Vaccin. https://doi.org/10.4161/hv.6.12.13143

974 Palsson-McDermott, E. M., Curtis, A. M., Goel, G., Lauterbach, M. A. R., Sheedy, F. J., Gleeson, L. E., …
975 O'Neill, L. A. J. (2015). Pyruvate Kinase M2 Regulates Hif-1α Activity and IL-1β Induction and Is a
976 Critical Determinant of the Warburg Effect in LPS-Activated Macrophages. *Cell Metabolism*,
977 *21*(1), 65–80. https://doi.org/10.1016/j.cmet.2014.12.005

978 Pasula, R., Martin, W. J., Kesavalu, B. R., Abdalla, M. Y., & Britigan, B. E. (2017). Passive transfer of
979 interferon-γ over-expressing macrophages enhances resistance of SCID mice to Mycobacterium
980 tuberculosis infection. *Cytokine*, *95*, 70–79. https://doi.org/10.1016/j.cyto.2017.02.009

981 Philips, J. A., & Ernst, J. D. (2012). Tuberculosis pathogenesis and immunity. *Annu Rev Pathol*, *7*, 353–
982 384. https://doi.org/10.1146/annurev-pathol-011811-132458

983 Potian, J. A., Rafi, W., Bhatt, K., McBride, A., Gause, W. C., & Salgame, P. (2011). Preexisting helminth
984 infection induces inhibition of innate pulmonary anti-tuberculosis defense by engaging the IL-4
985 receptor pathway. *Journal of Experimental Medicine*, *208*(9), 1863–1874.
986 https://doi.org/10.1084/jem.20091473

987 Quinn, S. M., Cunningham, K., Raverdeau, M., Walsh, R. J., Curham, L., Malara, A., & Mills, K. H. G.
988 (2019). Anti-inflammatory trained immunity mediated by helminth products attenuates the
989 induction of T cell-mediated autoimmune disease. *Frontiers in Immunology*, *10*(MAY).
990 https://doi.org/10.3389/fimmu.2019.01109

991 Quintin, J., Saeed, S., Martens, J. H. A., Giamarellos-Bourboulis, E. J., Ifrim, D. C., Logie, C., … Netea, M.
992 G. (2012). Candida albicans infection affords protection against reinfection via functional
993 reprogramming of monocytes. *Cell Host & Microbe*, *12*(2), 223–232.
994 https://doi.org/10.1016/j.chom.2012.06.006

995 Roy, S., Mukhopadhyay, D., Mukherjee, S., Moulik, S., Chatterji, S., Brahme, N., … Chatterjee, M.
996 (2018). An IL-10 dominant polarization of monocytes is a feature of Indian Visceral Leishmaniasis.
997 *Parasite Immunology*, *40*(7). https://doi.org/10.1111/pim.12535

998 Ryndak, M. B., & Laal, S. (2019). Mycobacterium tuberculosis Primary Infection and Dissemination: A
999 Critical Role for Alveolar Epithelial Cells. *Frontiers in Cellular and Infection Microbiology*, *9*, 299.
1000 https://doi.org/10.3389/fcimb.2019.00299

1001 Saeed, S., Quintin, J., Kerstens, H. H. D., Rao, N. A., Aghajanirefah, A., Matarese, F., … Stunnenberg, H.
1002 G. (2014). Epigenetic programming of monocyte-to-macrophage differentiation and trained
1003 innate immunity. *Science (New York, N.Y.)*, *345*(6204), 1251086.
1004 https://doi.org/10.1126/science.1251086

1005 Salgame, P., Yap, G. S., & Gause, W. C. (2013). Effect of helminth-induced immunity on infections with
1006 microbial pathogens. *Nature Immunology*. Nat Immunol. https://doi.org/10.1038/ni.2736

1007 Seth, P., Csizmadia, E., Hedblom, A., Vuerich, M., XIE, H., Li, M., … Wegiel, B. (2017). Deletion of lactate
1008 dehydrogenase-A in myeloid cells triggers antitumor immunity. *Cancer Research*,
1009 canres.2938.2016. https://doi.org/10.1158/0008-5472.CAN-16-2938

1010 Shi, L., Jiang, Q., Bushkin, Y., Subbian, S., & Tyagi, S. (2019). Biphasic dynamics of macrophage
1011 immunometabolism during Mycobacterium tuberculosis infection. *MBio*, *10*(2).
1012 https://doi.org/10.1128/mBio.02550-18

1013 Sica, A., Erreni, M., Allavena, P., & Porta, C. (2015). Macrophage polarization in pathology. *Cellular and*
1014 *Molecular Life Sciences*, *72*(21), 4111–4126. https://doi.org/10.1007/s00018-015-1995-y

1015 Van den Bossche, J., Baardman, J., Otto, N. A., van der Velden, S., Neele, A. E., van den Berg, S. M., …
1016 de Winther, M. P. J. (2016). Mitochondrial Dysfunction Prevents Repolarization of Inflammatory
1017 Macrophages. *Cell Reports*, *17*(3), 684–696. https://doi.org/10.1016/j.celrep.2016.09.008

1018 Van den Bossche, J., O'Neill, L. A., & Menon, D. (2017). Macrophage Immunometabolism: Where Are
1019 We (Going)? *Trends in Immunology*. https://doi.org/10.1016/j.it.2017.03.001

1020 van der Meer, J. W. M., Joosten, L. A. B., Riksen, N., & Netea, M. G. (2015). Trained immunity: A smart
1021 way to enhance innate immune defence. *Molecular Immunology*, *68*(1), 40–44.
1022 https://doi.org/10.1016/j.molimm.2015.06.019

1023 Viola, A., Munari, F., Sánchez-Rodríguez, R., Scolaro, T., & Castegna, A. (2019). The metabolic signature
1024 of macrophage responses. *Frontiers in Immunology*, *10*(JULY).
1025 https://doi.org/10.3389/fimmu.2019.01462

1026 Wang, F., Zhang, S., Vuckovic, I., Jeon, R., Lerman, A., Folmes, C. D., … Herrmann, J. (2018). Glycolytic
1027 Stimulation Is Not a Requirement for M2 Macrophage Differentiation. *Cell Metabolism*, *28*(3),

463-475.e4. https://doi.org/10.1016/j.cmet.2018.08.012

WHO. (2019). *Global Tuberculosis Report: Executive Summary 2019*. https://doi.org/WHO/CDS/TB/2019.23

Supplemental Information

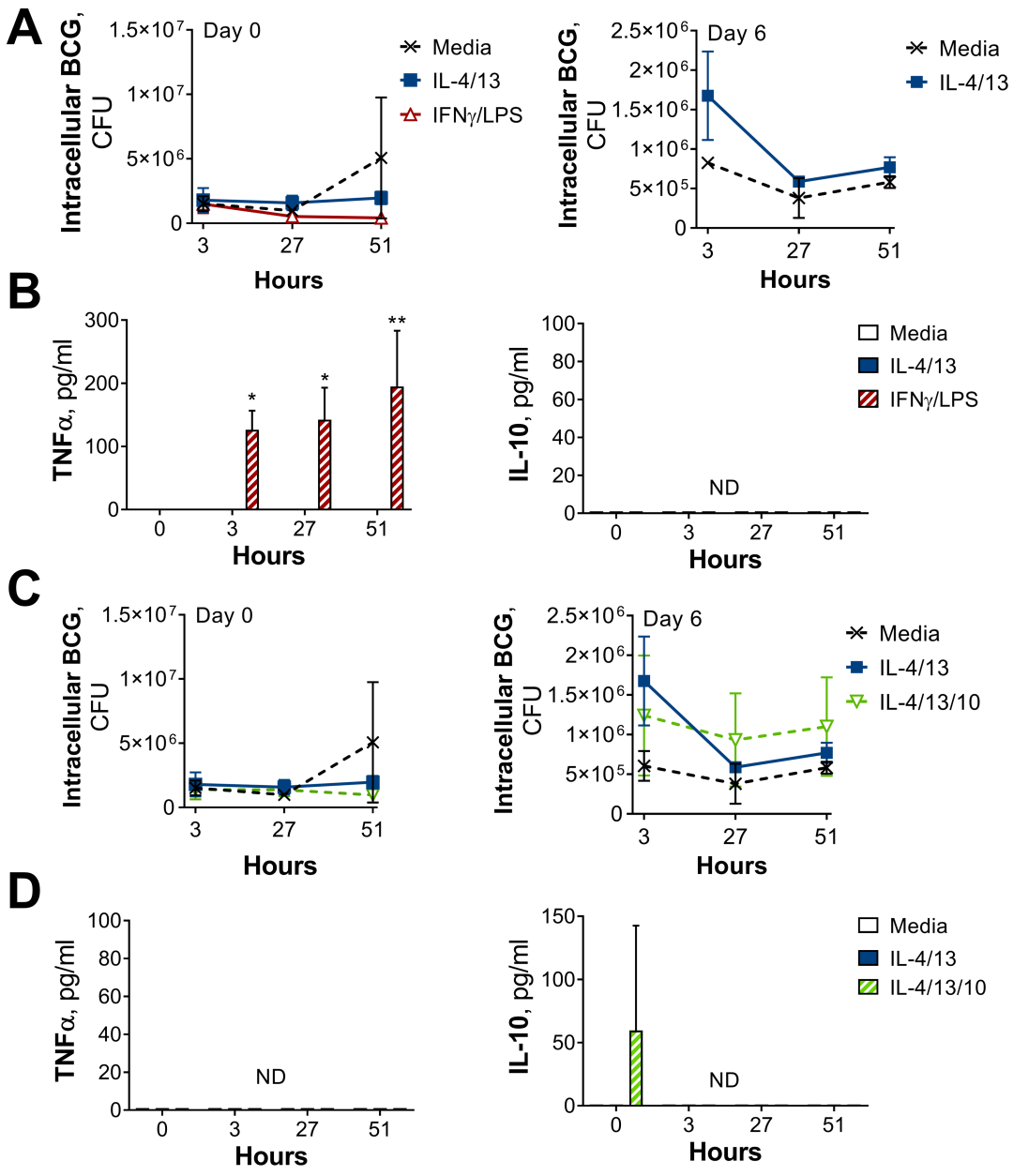

Figure S1. CFU counts and cytokine secretion from BCG killing experiments.

(**A-B**) BCG Denmark CFU counts (A) and cytokine secretion (B) on Day 0 or Day 6 after h following BMDM BCG infection. BMDMs were previously incubated with media control, IL-4 with IL-13 or IFNγ with LPS for 24 h on Day -1. Representative results (n = 2), standardized to 0.5×10^6 cells, shown as mean ± SEM (A-B) and analyzed by multiple t-test, with Holm-Sidak correction, compared with media control (B). (**C-D**) BCG Denmark CFU counts (C) and cytokine secretion (D) on Day 0 or Day 6 after h following BMDM BCG infection. BMDMs were previously incubated with media control or IL-4 and IL-13, with or without IL-10, for 24 h on Day -1. Representative results (n = 2), standardized to 0.5×10^6 cells, shown as mean ± SEM (C-D) and analyzed by multiple t-test, with Holm-Sidak correction, compared with media control (D). * $p \leq 0.05$, ** $p \leq 0.01$.

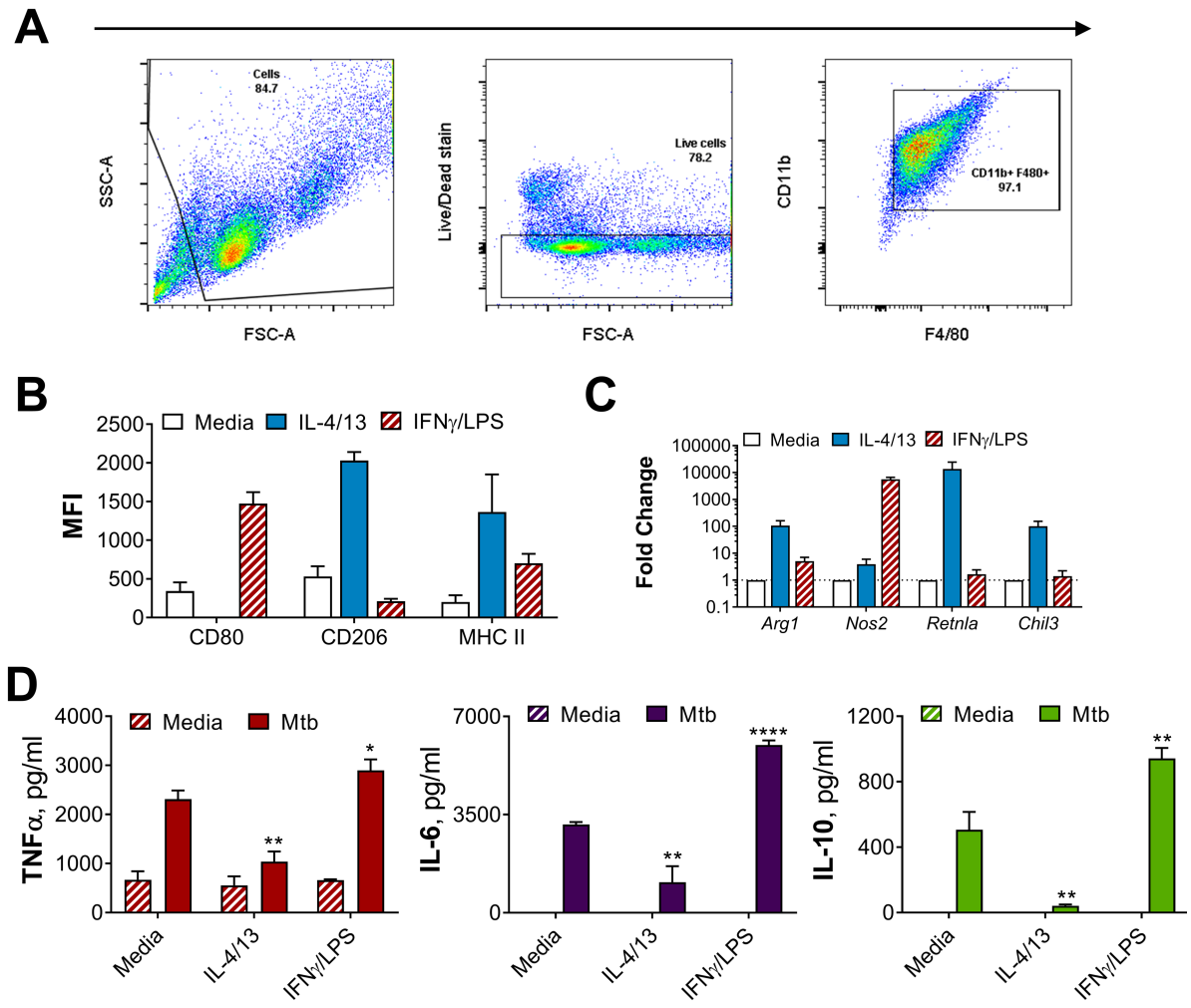

Figure S2. BMDMs either classically activated with IFNγ and LPS or alternatively activated with IL-4 and IL-13.

(**A**) Gating strategy for flow cytometry analysis, gating on cells, live cells and CD11b+ F480+ BMDMs. (**B**) Surface marker expression of CD80, CD206 and MHC II on BMDMs incubated with media as a control, IL-4 with IL-13 or IFNγ with LPS for 24 h (n = 3). (**C**) qPCR of indicated mRNA in BMDMs treated as in (B), standardized to media control (n = 4). (**D**) Cytokine secretion from BMDMs incubated with media, IL-4 with IL-13 or IFNγ with LPS for 24 h on Day -1 and stimulated with media or irradiated *M. tuberculosis* H37Rv (Mtb) for 24 h on Day 6 (n = 3). Mean ± SD are shown and analyzed by student's t-test, compared to media control. * $p \leq 0.05$, ** $p \leq 0.01$, *** $p \leq 0.001$, **** $p \leq 0.0001$.

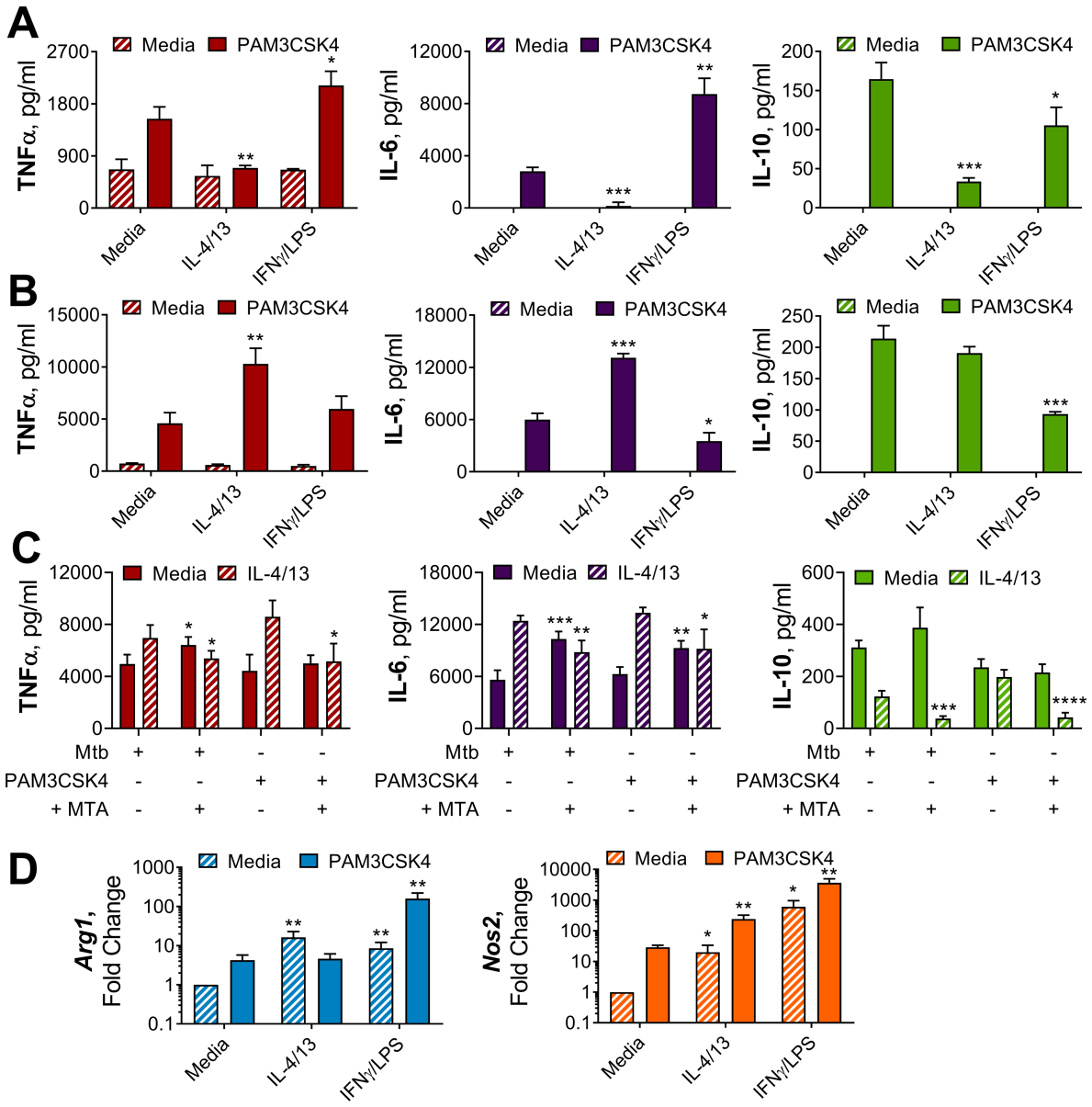

Figure S3. Methylation contributes to IL-4 and IL-13 innate training, which enhances inflammatory and bactericidal responses following TLR 1/2 and mycobacterial stimulation

(**A-B**) Cytokine secretion from BMDMs following incubation with media control, IL-4 with IL-13 or IFNγ with LPS for 24 h on Day -1 and incubated with media or PAM3CSK4 on Day 0 (A) or Day 6 (B) for 24 hours (n = 3). (**C**) Cytokine secretion following BMDM incubation with media control or IL-4 with IL-13 for 24 h on Day -1, with or without 1 hour pre-incubation with methylation inhibitor MTA, and incubation with irradiated *M. tuberculosis* H37Rv (Mtb) or PAM3CSK4 for 24 h on Day 6 (n = 4). (**D**) qPCR of indicated mRNA in BMDMs treated as in (B), standardized to BMDMs incubated with media Day -1 and Day 6 (n = 4). Mean ± SD are shown and analyzed by student's t-test, compared with media control (A-B, D) or comparing with or without MTA (C). * $p \leq 0.05$, ** $p \leq 0.01$, *** $p \leq 0.001$, **** $p \leq 0.0001$.

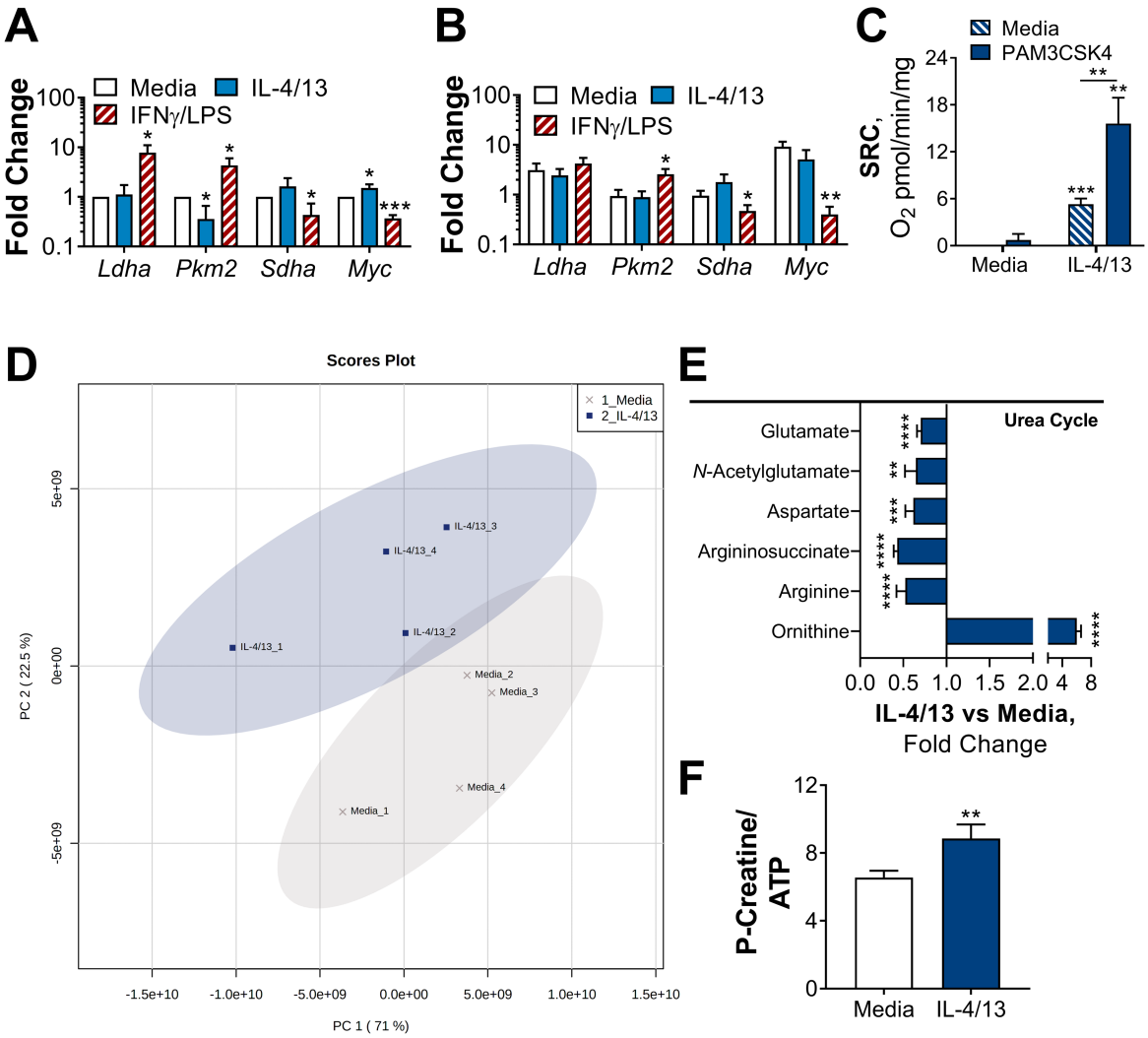

Figure S4. Challenged BMDMs previously trained with IL-4 and IL-13 retain M2-typical metabolism.

(**A-B**) qPCR of indicated mRNA in BMDMs following incubation with media control, IL-4 with IL-13 or IFNγ with LPS on for 24 h Day -1 and stimulated with media (A) or PAM3CSK4 (B) on Day 6 for 6 h (*Pkm2*) and 24 h (*Ldha, Sdha* and *Myc*). Fold change was standardized to BMDMs incubated with media Day -1 and Day 6 (n = 3). (**C**) Spare respiratory capacity (SRC) of BMDMs treated as in (A-B), with incubation of media or IL-4 with IL-13 on Day -1 (n = 3). (**D-F**) Metabolites isolated from BMDMs following incubation with either media control (untrained) or IL-4 with IL-13 (trained) for 24 h on Day -1 and stimulation with Mtb for 24 h on Day 6 (n = 4). Metaboanalyst principal component analysis (PCA) (D), fold change of metabolites from trained BMDMs compared with media control (=1) (E) and calculated ratio of phosphocreatine (P-creatine) to ATP (F) are shown. Mean ± SD are shown and analyzed by student t-test, compared with media control. * $p \leq 0.05$, ** $p \leq 0.01$, *** $p \leq 0.001$, **** $p \leq 0.0001$.

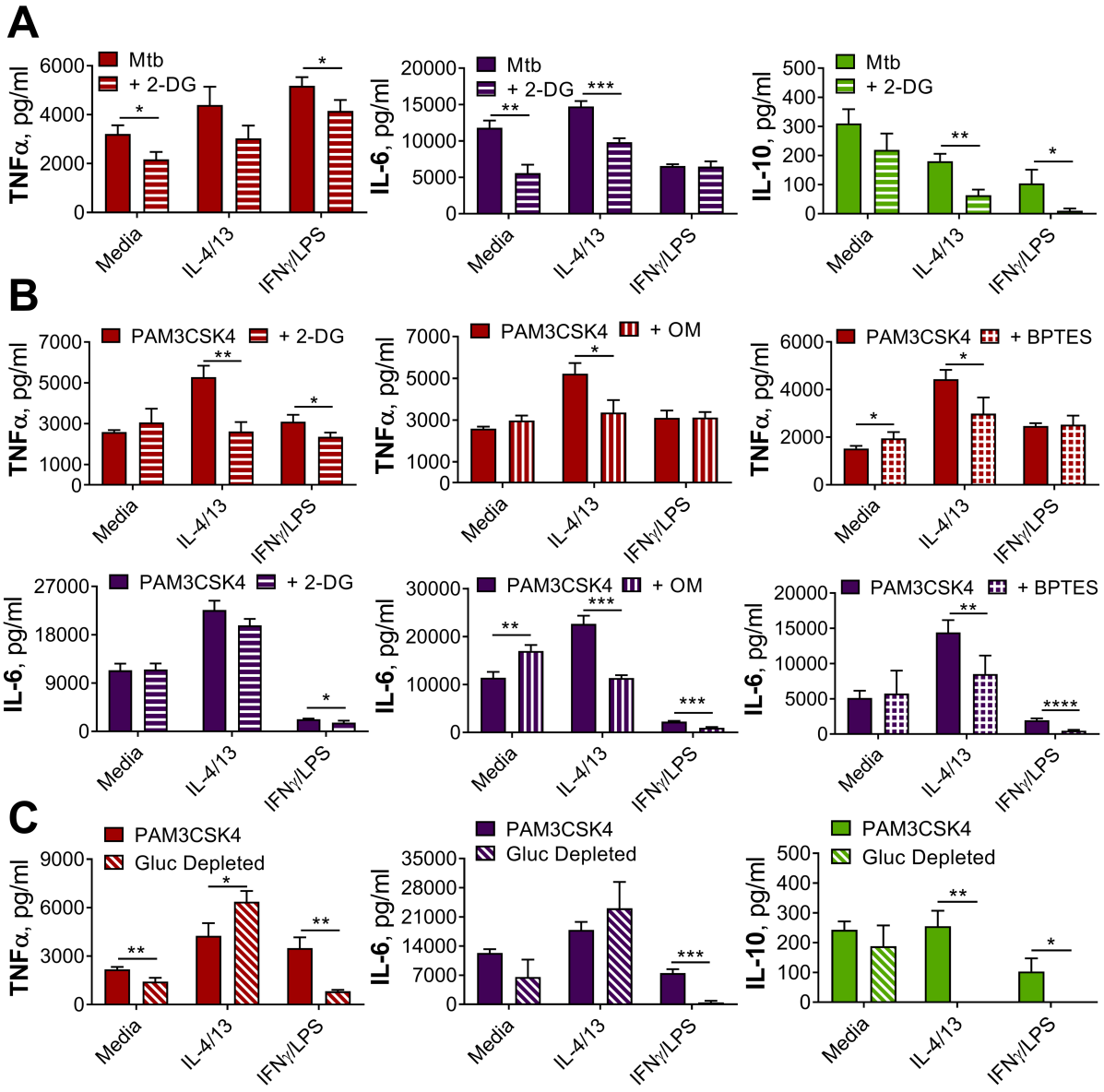

Figure S5. Innate training with IL-4 and IL-13 enhancement of pro-inflammatory responses is not dependent upon glucose metabolism.

(**A-B**) Cytokine secretion from BMDMs following incubation with media control, IL-4 with IL-13 or IFNγ with LPS for 24 h on Day -1 and incubation with irradiated *M. tuberculosis* H37Rv (Mtb) (A) or PAM3CSK4 (B) for 24 h on Day 6, with or without pre-incubation of metabolic inhibitors oligomycin (OM), 2-deoxy glucose (2-DG) or BPTES. (**C**) Cytokine secretion from BMDMs following incubation with media control, IL-4 with IL-13 or IFNγ with LPS for 24 h on Day -1 and incubation with media or PAM3CSK4 for 24 h on Day 6, with or without glucose depleted conditions between Day -1 to 7. Mean ± SD (n = 3-4) are shown and analyzed by student's t-test as indicated. * $p \leq 0.05$, ** $p \leq 0.01$, *** $p \leq 0.001$, **** $p \leq 0.0001$.

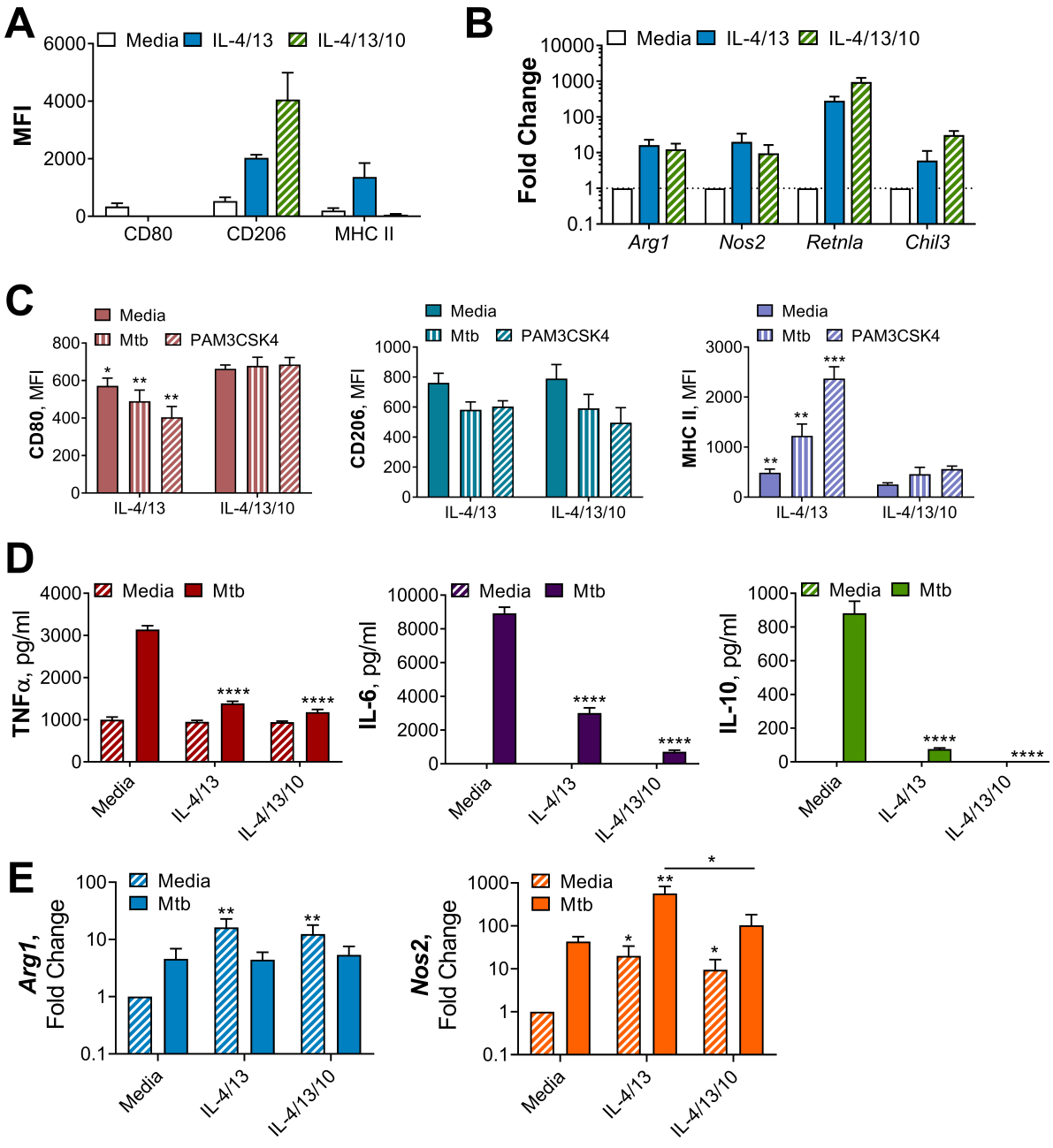

Figure S6. Alternative macrophage activation with or without IL-10.

(**A**) Surface marker expression of CD80, CD206 and MHC II on BMDMs incubated with media as a control or IL-4 and IL-13, with or without IL-10,D for 24 h (n = 3) (gating strategy shown Figure S2A). (**B**) qPCR of indicated mRNA in BMDMs treated as in (A), standardized to media control (n = 4). (**C**) Surface marker expression of CD80, CD206 and MHC II on BMDMs following incubation with IL-4 and IL-13, with or without IL-10, for 24 h on Day -1 and incubated with media, irradiated *M. tuberculosis* H37Rv (Mtb) or PAM3CSK4 for 24 h on Day 0 (n =3). (**D**) Cytokine secretion from BMDMs treated as in (C), incubated with media or Mtb for 24 h on Day 0 (n = 4). Mean ± SD (n = 4) are shown and analyzed by student t-test, compared with media control. (**E**) qPCR of indicated mRNA in BMDMs treated as in (C), incubated with media or Mtb for 24 h on Day 0, standardized to BMDM incubated with media on Day -1 and Day 0 (n = 4). Mean ± SD (n = 4) are shown (A-E) and analyzed by student's t-test, compared with media control (D-E), comparing with or without IL-10 (C, E). * $p \le 0.05$, ** $p \le 0.01$, *** $p \le 0.001$, **** $p \le 0.0001$.

1116 **Table S 1. Primer sequences for reverse transcription PCR.**

Primer		Source
Actb (RefSeq: NM_007393.5)	FP: GCTTCTTTGCAGCTCCTTCGT RP: CGTCATCCATGGCGAACTG	Invitrogen Custom DNA Oligos
Arg1 (RefSeq: NM_007482.3)	FP: TACAAGACAGGGCTCCTTTCAG RP: TGAGTTCCGAAGCAAGCCAA	Invitrogen Custom DNA Oligos
Chitl3 (RefSeq: NM_009892.3)	FP: AAGCTCTCCAGAAGCAATCC RP: AGAAGAATTGCCAGACCTGTGA	Invitrogen Custom DNA Oligos
Ldha (RefSeq: NM_010699.2, NM_001136069.2)	FP: GAGACTTGGCTGAGAGCATAA RP: GATACATGGGACACTGAGGAA	Eurofins genomics (MWG)
Myc (RefSeq: NM_010849.4)	FP: CAGCGACTCTGAAGAAGAGCA RP: GACCTCTTGGCAGGGGTTTG	Invitrogen Custom DNA Oligos
Nos2 (RefSeq: NM_010927.4, NM_001313921.1, NM_001313922.1)	FP: TCCTGGACATTACGACCCCT RP: CTCTGAGGGCTGACACAAGG	Invitrogen Custom DNA Oligos
Pkm2 (RefSeq: NM_011099.4, NM_001378868.1, NM_001378869.1, NM_001378870.1)	FP: TGTCTGGAGAAACAGCCAAG RP: CGAATAGCTGCAAGTGGTAGA	Eurofins genomics (MWG)
Retnla (RefSeq: NM_020509.3)	FP: CAGCTGATGGTCCCAGTGAAT RP: AGTGGAGGGATAGTTAGCTGG	Invitrogen Custom DNA Oligos
Sdha (RefSeq: NM_023281.1)	FP: GGAACACTCCAAAAACAGACC RP: CCACCACTGGGTATTGAGTAGAA	Eurofins genomics (MWG)
Tbp (RefSeq: NM_013684.3)	FP: CAGGAGCCAAGAGTGAAGAACA RP: AAGAACTTAGCTGGGAAGCCC	Invitrogen Custom DNA Oligos

1117